Vibronic coupling explains the ultrafast carotenoid-to-bacteriochlorophyll energy transfer in natural and artificial light harvesters

Václav Perlík, Joachim Seibt, Laura J. Cranston, Richard J. Cogdell, Craig N. Lincoln, Janne Savolainen, František Šanda, Tomáš Mančal, and Jürgen Hauer

Citation: The Journal of Chemical Physics **142**, 212434 (2015); doi: 10.1063/1.4919548
View online: http://dx.doi.org/10.1063/1.4919548
View Table of Contents: http://scitation.aip.org/content/aip/journal/jcp/142/21?ver=pdfcov
Published by the AIP Publishing

Vibronic coupling explains the ultrafast carotenoid-to-bacteriochlorophyll energy transfer in natural and artificial light harvesters

Václav Perlík,[1] Joachim Seibt,[1] Laura J. Cranston,[2] Richard J. Cogdell,[2] Craig N. Lincoln,[3] Janne Savolainen,[4] František Šanda,[1] Tomáš Mančal,[1] and Jürgen Hauer[3,a)]
[1]*Institute of Physics, Faculty of Mathematics and Physics, Charles University in Prague, Ke Karlovu 5, Prague 121 16, Czech Republic*
[2]*Institute of Molecular Cell and System Biology, College of Medical, Veterinary and Life Sciences, University of Glasgow, Glasgow Biomedical Research Centre, 120 University Place, Glasgow G12 8TA, Scotland*
[3]*Photonics Institute, Vienna University of Technology, Gusshausstrasse 27, 1040 Vienna, Austria*
[4]*Department of Physical Chemistry II, Ruhr-University Bochum, 44780 Bochum, Germany*

(Received 5 February 2015; accepted 20 April 2015; published online 4 May 2015)

The initial energy transfer steps in photosynthesis occur on ultrafast timescales. We analyze the carotenoid to bacteriochlorophyll energy transfer in LH2 *Marichromatium purpuratum* as well as in an artificial light-harvesting dyad system by using transient grating and two-dimensional electronic spectroscopy with 10 fs time resolution. We find that Förster-type models reproduce the experimentally observed 60 fs transfer times, but overestimate coupling constants, which lead to a disagreement with both linear absorption and electronic 2D-spectra. We show that a vibronic model, which treats carotenoid vibrations on both electronic ground *and* excited states as part of the system's Hamiltonian, reproduces all measured quantities. Importantly, the vibronic model presented here can explain the fast energy transfer rates with only moderate coupling constants, which are in agreement with structure based calculations. Counterintuitively, the vibrational levels on the carotenoid electronic ground state play the central role in the excited state population transfer to bacteriochlorophyll; resonance between the donor-acceptor energy gap and the vibrational ground state energies is the physical basis of the ultrafast energy transfer rates in these systems. © *2015 AIP Publishing LLC.* [http://dx.doi.org/10.1063/1.4919548]

I. INTRODUCTION

Modern researchers have been fascinated by how efficiently solar photons are converted into chemical energy in photosynthesis. Initially, photons are absorbed in so-called light-harvesting complexes (LHCs). The following steps of the cascading energy transfer within LHCs are remarkably efficient: at low light intensities, 9 out of 10 absorbed photons create a charge separated state in the reaction center as the basis for further energy conversion.[1,2] A thorough understanding of this process and its technological utilization will be a major contribution to a sustainable energy concept. Accordingly, this hope has motivated numerous studies with the aim of finding and characterizing bio-inspired, artificial light harvesting systems.[3] Despite the efforts, bio-mimetic systems remain still less efficient and less stable than their natural counterparts. It is generally accepted that a detailed picture of the involved electronic energy levels as well as the energy dissipation pathways in both artificial and natural light harvesters is crucial in the realization of an efficient and durable bio-mimetic photosystem.

While there is great structural diversity and flexibility in photosynthetic LHCs,[4] essentially only two molecular species serve as pigments, namely, carotenoids and (bacterio)chlorophylls, (B)Chls. Carotenoids and (B)Chls are fundamentally different in structure and complementing in physiological function. Carotenoids are linear molecules with varying endgroups. Their optical properties are defined by the π-conjugated electronic states, extended along the polyene backbone as depicted in Fig. 1. The earliest suggested energy flow models used a three-level system with ground state S_0 and excited states S_2 and S_1.[5] The linear absorption spectra of carotenoids stem from transitions between the electronic ground state S_0 and the "bright" electronic excited state S_2, whereas the lowest-lying excited state S_1 is "dark," with the $S_0 \rightarrow S_1$ transition being one-photon forbidden. The properties of S_1 are observed either by two-photon absorption from S_0 or by using nonlinear spectroscopy, e.g., transient absorption (TA), where the excited state absorption (ESA) $S_1 \rightarrow S_n$ is characteristically strong.[5] The population flow rate from S_2 and S_1 strongly depends on the carotenoid's chain length, with typical transfer times of less than 200 fs for solvated carotenoids (*in vitro*). The role of possible intermediate states, at energies between those of S_2 and S_1, was controversially discussed in the literature and reviewed by Polivka and Sundstrom.[6] With respect to the carotenoid to BChl energy transfer, such an intermediate state termed S_x was recently suggested to be responsible for up to 50% of the overall transfer efficiency.[7,8] The discussion relates to theoretical works by Tavan and Schulten,[9] predicting additional states with $1B_u^-$ and $3A_g^-$ symmetry besides S_2 ($1B_u^+$) and S_1 ($2A_g^-$).

a)Author to whom correspondence should be addressed. Electronic mail: juergen.hauer@tuwien.ac.at

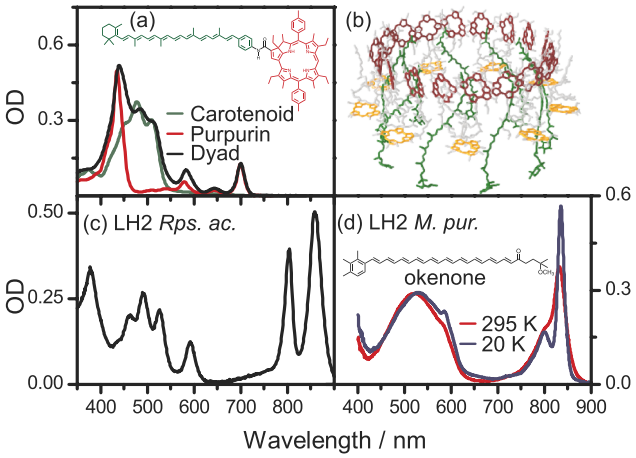

FIG. 1. (a) Absorption spectra and molecular structure of the carotenopurpurin dyad (black line) and its constituting carotenoid (donor, green) and porphyrinic acceptor in red. (b) Structural model and absorption spectrum (c) of LH2 *Rps. ac.* (d) Absorption spectra at different temperatures of LH2 *M. pur.*, along with the molecular structure of the bound carotenoid (okenone).

In an idealized C_{2h}-symmetry, these additional states will be optically dark with respect to the ground state S_0 ($1A_g^-$). Despite their dipole forbidden character, the energetic position of the $1B_u^-$ and $3A_g^-$ states will depend on carotenoid's chain length. For nine conjugated double bounds as found for the carotenoids studied in this work, the $3A_g^-$ state can be neglected due to its high energy. The $1B_u^-$ state, however, comes to lie between S_2 ($1B_u^-$) and S_1 ($2A_g^-$). Despite its intermediate energetic position, the discussion about an actual involvement of the $1B_u^-$ state in the energy deactivation network of carotenoids is still ongoing, with arguments for[7,8,10–14] and against it.[15–18]

Besides quenching of harmful long-lived triplet states in (B)Chls and structural support of LHCs, the efficient transfer of the excitation energy from carotenoid to the lower lying (B)Chl states is the main functional role of carotenoids. The most efficient transfer route occurs from carotenoid's S_2 state to the energetically closest (B)Chl-state, namely, Q_x. Transfer from S_1 to Q_y is found in several antenna complexes and occurs on a longer timescale than $S_2 \rightarrow Q_x$.[5] *In vivo*, i.e., as part of a LHC, the lifetime of S_2 decreases dramatically.[19] For example, in LHCII, the main antenna system of higher plants and algae, the lifetime of the S_2 state of the involved carotenoids is ~120 fs *in vitro* and only ~26 fs *in vivo* as measured by fluorescence upconversion, which makes it one of the shortest in naturally occurring systems.[20] The reason for this dramatic decrease in carotenoid lifetime is the interaction with the closely neighboring (B)Chls. Chemically, the chromophore of (B)Chls is a nitrogen containing tetrapyrrole-macrocycle with one or two reduced pyrrole rings. According to the four orbital picture of porphyrins,[21] the absorption spectrum of (B)Chls is described by at least two transitions in the so-called Soret band (B_x and B_y for HOMO - LUMO+1 and HOMO-1 - LUMO+1, respectively) and two Q-band transitions (HOMO - LUMO for Q_y and HOMO-1 - LUMO for Q_x). Depending on molecular structure, the B-band is found in the blue to near-UV spectral region. The Q-bands stem from transitions with orthogonal transition dipole moments and are energetically degenerate for planar and symmetric porphyrins such as metal-centered phthalocyanines.[22,23] (B)Chls show a reduced symmetry in comparison, causing a split of the Q-band. For BChl *a* in organic solvents, the Q_x-band peaks near 600 nm, while the maximum of Q_y is found just below 800 nm. Despite their structural differences, carotenoids and (B)Chls fulfill complementary tasks in photosynthetic antenna complexes. *In vivo*, excitonic coupling and the polar protein environment shift the Q_y-band of (B)Chls to the red, thus covering the red edge of the visible solar spectrum.

In this contribution, we investigate an artificial dyad that mimics *Rhodopseudomonas acidophila* (LH2 *Rps. ac.*), and compare it to a naturally abundant LH2 of *Marichromatium purpuratum* (LH2 *M. pur.*, formerly known as *Chromatium purpuratum*). The main difference between the artificial dyad and LH2 *M. pur.* is the smaller energy difference between S_2 and Q_x in the latter. Based on this comparison, along with results reported in the literature for LH2 *Rps. ac.*, we develop a novel energy transfer model for $S_2 \rightarrow Q_x$ energy transfer. We show that a transfer process mediated by vibronic resonances between S_2 and Q_x presents a mechanistic alternative to conventional schemes incorporating only electronic coupling. In particular, the carotenoid vibrational levels in its electronic ground state are crucial in establishing the resonance between the carotenoid and BChl transitions.

II. MATERIALS AND METHODS

A. Sample preparation

The dyad-sample was provided by Professor Ana Moore and synthesized according to previously published procedures.[24,25] The dyad and its constituents, i.e., the dyad-carotenoid as the energy donor and purpurin as the acceptor, were dissolved in spectroscopic grade toluene.

Cells of *Marichromatium purpuratum* strain BN5500 (also designated DSM1591 or 984) were grown anaerobically in the light, harvested by centrifugation and suspended in 20 mM tris–HCl pH 8.0. Then, upon the addition of DNase and $MgCl_2$, the cells were broken by passage through a French press. The photosynthetic membranes were collected from the broken-cell mixture by centrifugation and resuspended in the tris–HCl solution to an optical density (OD) of 0.6 at 830 nm. The membranes were then solubilized by the addition of 1%(v/v) of the detergent N, N-dimethyldodecylamine-N-oxide lauryldimethylamine-N-oxide (LDAO). These solubilized membranes were subjected to sucrose density centrifugation with a step gradient (as described previously by Brotosudarmo *et al.*[26]) in order to fractionate the sample into LH2 and RC–LH1 complexes. The LH2 fraction was then further purified by ion-exchange chromatography using diethylaminoethyl cellulose (DE52, Whatman). The bound protein was washed with 20 mM tris–HCl pH 9.0 containing 0.15% dodecyl maltoside (DM) to exchange the LDAO detergent and then eluted by adding increasing concentrations of NaCl also containing 0.15% DM. Additional purification was achieved by gel-filtration chromatography using a Superdex S-200 column (XK 16/100, GE Healthcare) which had been equilibrated overnight with 20 mM tris–HCl pH 9.0 plus 0.15% DM.

B. Time resolved spectroscopy

The two spectroscopic techniques employed in this article, transient grating (TG) and two dimensional electronic spectroscopy (2D-ES) are both four wave mixing techniques. In four wave mixing, three excitation pulses interact with the sample to create a non-linear polarization of third order in the field, which acts as a source term for an emerging signal. In the experiment employed here, all three excitation fields emerge along individual wavevectors, resulting in a non-linear signal direction which is different from any of the incoming beams. This allows for a virtually background free signal. Details of the experimental layout are given elsewhere.[27,28] Briefly, excitation pulses tunable throughout the visible spectral range are provided by a home-built noncollinear optical parametric amplifier (NOPA),[29] pumped by a regenerative titanium-sapphire amplifier system (RegA 9050, Coherent, Inc.) at 200 kHz repetition rate. Pulse spectra were chosen to overlap with the investigated sample's absorption spectrum (see Fig. 1) and compressed down to a temporal FWHM of sub-11 fs in each case, determined by intensity autocorrelation. The pulses were attenuated by a neutral density filter to yield 8.5 nJ per excitation pulse at the sample. This corresponds to a fluence of less than 3.0×10^{14} photons/cm^2 per pulse. The four wave mixing experiment used for both TG and 2D-ES relies on a passively phase stabilized setup with a transmission grating[30,31] and has a temporal resolution of 5.3 as for t_1, i.e., the delay between the first two pulses and 0.67 fs for t_2, the delay between second and third excitation pulse. A detailed description was given by Milota *et al.*[32] For TG measurements, t_1 was kept at 0 fs while t_2 was scanned. The emerging signal was spectrally resolved in ω_3 by a grating-based spectrograph and recorded with a CCD camera. At a given delay time, spectra were not recorded on a shot-to-shot basis, but averaged over approximately 10^5 shots per spectrum. Sample handling was accomplished by a wire-guided drop jet[33] with a flow rate of 20 ml/min and a film thickness of approximately 200 μm. The fact that the jet operates without the use of cell windows allows us to interpret 2D spectra and TG-signals even during pulse overlap ($t_1 = t_2 = 0$). All measurements were performed under ambient temperatures (295 K).

C. Modeling

1. Modeling of 2D-spectra

To facilitate the interpretation of the measured 2D-spectra, we analyzed the spectra quantitatively. It turned out that simulations including only carotenoid can explain most features of the measured 2D spectra. Therefore, the model was based on the properties of the carotenoid component, whereas transfer from carotenoid to BChl only entered in terms of a contribution to lifetime broadening. It was assumed that the spectral profile of the pulses used in the experiment allows for resonant transitions between S_0 and S_2, and from S_1 to S_n subsequent to population transfer from S_2 to S_1. With respect to a possible involvement of intermediate states such as $1B_u^-$ and its role in carotenoid to bacteriochlorophyll energy transfer,[7] we note that Marek *et al.*[13] used a four wave mixing sequence after an initial pump pulse (Pump-DFWM) to extract information about vibrational wavepacket motion as a function of delay time between the initial pump pulse and the first pulse of the FWM-sequence. The authors observed a long lived, strongly oscillatory feature peaking at 40 fs initial pump delay. It was argued that such a delayed stimulated emission (SE) maximum is best explained by an intermediate state between S_2 and S_1. The vibrational modes retrieved from this intermediate state are qualitatively identical to those found on S_1 or S_2.[18] For the purposes of our work, this means that even if S_x mediates part of the carotenoid to bacteriochlorophyll energy transfer, it will do so via the same set of vibrational modes as S_2. Hence, a possible involvement of S_x will not affect our argumentation focusing on the role of vibrations in electronic energy transfer. Vibrational modulation of electronic transitions is modelled by assuming spectral density $J(\omega)$ or, equivalently, the corresponding lineshape function $g(t)$ connected by a general formula,[34]

$$g(t) = \frac{1}{2\pi}\int_{-\infty}^{\infty} d\omega \frac{1-\cos(\omega t)}{\omega^2} \coth\left(\frac{\omega}{2k_B T}\right) J(\omega) + \frac{i}{2\pi}\int_{-\infty}^{\infty} d\omega \frac{\sin(\omega t)-\omega t}{\omega^2} J(\omega). \quad (1)$$

Transition between S_0 and S_2 is modulated by two undamped oscillators

$$J_{UO,kl,i}(\omega) = \pi\omega\lambda_{UO,kl,i}\left[\delta(\omega-\omega_{UO,i}) + \delta(\omega+\omega_{UO,i})\right], \quad (2)$$

with reorganization energies $\lambda_{UO,i}$, $i \in \{1,2\}$ and vibrational frequencies $\omega_{UO,i}$, $i \in \{1,2\}$. The reorganization energies are connected to the Huang-Rhys (HR) factors $\chi_{UO,kl,i}$ via $\lambda_{UO,kl,i} = \chi_{UO,kl,i}\omega_{UO,i}$.

Vibrations modulating the S_1 state of the carotenoid are damped. We retain the results of the spin boson model and assume the spectral density for two weakly damped harmonic oscillators in a form

$$J_{UO,kl,i}(\omega) = 2\lambda_{UO,kl,i}\omega_{UO,i}^2 \frac{\omega\gamma_{UO,kl,i}}{(\omega_{UO,i}^2-\omega^2)^2 + \omega^2\gamma_{UO,kl,i}^2}, \quad (3)$$

where $\gamma_{UO,kl,i}$ is the oscillation damping rate. Furthermore, influence of the solvent or protein environment was described by two overdamped Brownian oscillator spectral density components with damping constants $\Lambda_{kl,i}$, $i \in \{1,2\}$ and reorganization energies $\lambda_{BO,kl,i}$, $i \in \{1,2\}$[34]

$$J_{BO,kl,i}(\omega) = 2\lambda_{BO,kl,i}\frac{\omega\Lambda_{kl,i}}{\omega^2+\Lambda_{kl,i}^2}. \quad (4)$$

The sum of all line shape function components was included in the response functions for the calculation of 2D-spectra. The response functions contain the transition frequencies ω_{kl} between the electronic states k and l and rate constants of transfer processes. Besides the rate $k_{S_2\to S_1}$ for transfer from S_2 to S_1, also a transfer rate $k_{S_2\to Q_x}$ from S_2 to an electronic state Q_x of the chlorophyll component of the LH2 complex plays a role in lifetime broadening effects.

The rate of lifetime broadening in S_2 is given by a dephasing rate Γ_{S_2} which reads as

$$\Gamma_{S_2} = \frac{1}{2}(k_{S_2\to S_1} + k_{S_2\to Q_x}). \quad (5)$$

For lifetime broadening in S_1, a rate Γ_{S_1} was introduced. The response functions can be distinguished by their rephasing or nonrephasing properties and assigned to excitation processes of SE, ground state bleaching (GSB), or ESA type, where in the case of SE and GSB, only the electronic transition dipole moment $\mu_{S_0S_2}$ enters, while for ESA components with population transfer, the transition dipole moment $\mu_{S_1S_n}$ also appears.

The response functions were formulated in analogy to Refs. 35 and 36 and are given in the Appendix. The sum of all rephasing and nonrephasing response function components yields the third-order response $S_R^{(3)}(\tau_3,\tau_2,\tau_1)$ and $S_{NR}^{(3)}(\tau_3,\tau_2,\tau_1)$, respectively, which reflect the excitation dynamics in the limit of infinitely short pulses. The influence of finite excitation pulse width was taken into account in analogy to Ref. 37, i.e., by convolution of the calculated signal with the pulses. By integration over the time intervals τ_1, τ_2, and τ_3 between the electronic transitions, the resulting third-order polarization is transformed into a dependence on the pulse delays t_1, t_2, and t_3. The rephasing part of the 2D-spectrum is obtained via

$$\sigma_{2D,R}(\omega_1,t_2,\omega_3) = \int_0^\infty dt_1 \int_0^\infty dt_3 \exp(-i\omega_1 t_1) \times \exp(i\omega_3 t_3) P_R^{(3)}(t_1,t_2,t_3); \quad (6)$$

the nonrephasing part results from

$$\sigma_{2D,NR}(\omega_1,t_2,\omega_3) = \int_0^\infty dt_1 \int_0^\infty dt_3 \exp(i\omega_1 t_1) \times \exp(i\omega_3 t_3) P_{NR}^{(3)}(t_1,t_2,t_3). \quad (7)$$

2. Calculation of energy transfer rate in a vibronic model

To simulate the energy transfer rate from the carotenoid S_2 state to the Q_x of the BChl in LH2 and the dyad, we employ a vibronic hetero-dimer model. This approach is natural for the dyad showing no signs of aggregation between the chromophores. For LH2, the monomeric treatment of Q_x and S_2 is also justified, given that there are no signs of excitonic splitting for these bands. Moreover, the carotenoid predominantly interacts with one of its neighboring B850 BChls with the next nearest neighbor coupling showing only half the interaction strength.[38]

To model the carotenoid molecule, we use an effective two state model which involves two electronic states (S_0 and S_2) and one effective vibrational mode which replaces the two fast vibrational modes with frequencies $\Omega_1 \approx 1150$ cm^{-1} and $\Omega_2 \approx 1500$ cm^{-1} known to be present in the carotenoid. The effective mode simulates the progression of states $|0\rangle_{1500}|0\rangle_{1150}$, $|0\rangle_{1500}|1\rangle_{1150}$, $|1\rangle_{1500}|0\rangle_{1150}$, $|0\rangle_{1500}|2\rangle_{1150}$, $|1\rangle_{1500}|1\rangle_{1150}$, $|2\rangle_{1500}|0\rangle_{1150}$, ... which originates from the two modes. We can order these levels into groups with vibrational energies approximately equal to the values corresponding to a progression of a single oscillator with the average vibrational energy, i.e. to 0, ≈1325 cm^{-1}, ≈2650 cm^{-1}, etc. (counted from the zero point energy). Because the spectral lines corresponding to the transitions to the states listed above are broadened, they act effectively as one mode with an average frequency and an effective HR-factor. This carotenoid mode (referred to as primary mode further on in this paper) is coupled to a bath of harmonic oscillators[39–41] (a secondary mode or a secondary bath) which provides damping and dephasing. The coupling between the primary mode and the carotenoid electronic transition provides the optical dephasing leading to the broadening of the absorption spectra. In order to calculate correctly the energy transfer rate, we parametrize the primary mode and its coupling to the bath of secondary harmonic oscillators in such a way that it reproduces absorption spectra. Fitting the carotenoid absorption spectrum with a single effective mode (Fig. 6) leads to qualitatively good agreement with experiment, showing that the vibrational modulation of the $S_0 \rightarrow S_2$ transition can be very well represented by a single primary mode. This effective model of the bath enables us to limit the bath description to one harmonic mode whose dynamics is treated explicitly by a master equation according to Ref. 39. In this way, the primary mode effectively provides a correct bath spectral density for the energy transfer between the carotenoid and BChl while allowing for a non-perturbative treatment. A fit of the absorption spectrum of the carotenoid in the dyad yields the carotenoid effective vibrational frequency $\omega_{\text{eff}} = 1390$ cm^{-1}, HR factor $s_{\text{eff}} = 1.3$, the reorganization energy of the secondary bath $\lambda_b = 670$ cm^{-1}, and the bath correlation time $\tau_b = 30$ fs. For the LH2 *M. pur.*, we obtained $\omega_{\text{eff}} = 1453$ cm^{-1}, $s_{\text{eff}} = 1.21$, $\lambda_b = 1242$ cm^{-1}, and $\tau_b = 54$ fs.

The Q_x states of the BChl (LH2 *M. pur.*) and purpurin (the dyad) are treated by the same model. The primary mode on BChl and purpurin are chosen to fit the respective absorption spectrum including the significant vibrational side bands. The side band for the purpurin can be easily located in the monomeric absorption spectrum given in Fig. 1. By fitting the purpurin monomeric absorption spectrum, we get the effective mode frequency $\omega_{purp} = 1246$ cm^{-1}, HR factor $s_{purp} = 0.61$, reorganization energy $\lambda_{purp} = 600$ cm^{-1}, and bath correlation time of $\tau_{purp} = 47$ fs. BChl absorption spectrum exhibits a much weaker vibrational side band and leads to a smaller HR factor of $s_{BChl} = 0.22$. Other parameters are as follows: $\omega_{BChl} = 1284$ cm^{-1}, $\lambda_{BChl} = 1911$ cm^{-1}, and $\tau_{BChl} = 100$ fs. The effective vibrational modes represent the overdamped part of the spectral density found in BChls (see, e.g., Ref. 42) by the term discussed in Sec. IV B 2 and the side band by its first replica. The strength of this replica is given by the HR factor.

The parameters obtained by the fit of the monomers are slightly readjusted in a fit of the aggregate spectra, either the purpurin-carotenoid dyad or the LH2 complex. Energy transfer rates are then estimated with no further adjustment of the parameters. To determine the energy transfer rate, the population dynamics of the system is calculated by the master equation from Ref. 41. The population transfer time $\tau_{S_2 \rightarrow Q_x}$ is defined as the time it takes for the S_2-population, initially set to 1, to decrease to $1/e \approx 0.368$.

III. RESULTS

A. Absorption

Fig. 1(a) shows the absorption spectrum of the dyad (black) and its constituents, i.e., the carotenoid donor (green) and the purpurin acceptor (red).

Details on the dyad's structure and dynamics are given in detail elsewhere.[24,25,43,44] It is a donor-acceptor system,

consisting of a β-carotene derivative (donor, green in the molecular structure in Fig. 1(a)), and a tetrapyrrole-macrocycle as an acceptor, referred to as purpurin (red). The dyad-carotenoid and purpurin are linked by an amide bond, providing structural rigidity but only partial conjugation between donor and acceptor. The dyad was synthesized to mimic LH2 *Rps. ac.*, whose structure is depicted in Fig. 1(b), as taken from the Papiz *et al.*[45] LH2 *Rps. ac.* consists of nine pairs of pigment-protein subunits (α/β-subunits), forming two concentric cylinders, to which carotenoids and BChl *a* molecules are bound non-covalently. As can be seen in Fig. 1(b), the BChls are arranged in two ring-like structures (red and yellow) with different numbers of BChls (18 for red and 9 for yellow) and ring diameters, leading to a weakly and strongly interacting set of BChls (yellow and red, respectively). As a result, the excitonic part of the absorption spectrum of LH2 *Rps. ac.*, shown in Fig. 1(c), exhibits two peaks, one near the monomeric Q_y-transition at 800 nm and a red-shifted peak near 850 nm. The red and yellow sets of BChls in Fig. 1(b) are, therefore, referred to as B850 and B800, respectively. The carotenoid is in van der Waals contact (<3.5 Å) with both the B800 and the B850 rings.[45,46] The dyad lacks such excitonic bands, as its structure is monomeric and there are no interacting BChl-moieties. An interesting difference between the absorption spectrum of the dyad and LH2 *Rps. ac.* arises in the carotenoid region of the spectrum. The vibronic structure of the monomeric carotenoid's absorption spectrum, shown in green in Fig. 1(a), is more pronounced than in the dyad, shown in black. This can be understood by invoking vibronic coupling between donor and acceptor, as will be addressed in detail in Sec. IV.

The absorption spectrum of LH2 *M. pur.* (Fig. 1(d)) exhibits substantially less vibronic modulation in carotenoid region of the spectrum. This is attributed to the disorder induced by polar endgroup of the bound carotenoid (okenone), interacting strongly with the polar *in vivo* protein environment. As the bright S_2-state carries ionic character,[9] its energy relative to S_0 is strongly affected by the interaction with the protein and shifts to the red in comparison the carotenoid (rhodopin glucoside) of LH2 *Rps. ac.* The BChl *a* molecules in LH2 *M. pur.* do not show similar bathochromic shifts, which lead to a greatly enhanced overlap of the carotenoid- and Q_x-band in this system. The excitonic region of the spectrum of LH2 *M. pur.* exhibits a less pronounced red shift with respect to the monomeric transition as compared to LH2 *Rps. ac.* Recent preliminary X-ray structure analysis[47] explains this by a reduced number of α/β-subunits (eight for LH2 *M. pur.* and nine in the case of LH2 *Rps. ac.*).

B. Transient grating

Fig. 2(a) shows the emission frequency (ω_3) resolved TG signal of LH2 *M. pur*. The signal shows a broad frequency range, spanning the entire spectrum of the excitation pulse, shown as an orange line in Fig. 2(b), in comparison to the absorption spectrum of LH2 *M. pur*. depicted as a grey area. The double-peaked structure of the excitation spectrum explains the overall shape of the TG-signal. The dashed lines mark frequencies characteristic for S_2 (dashed green line) and Q_x (dashed dark red line). Figures 2(c) and 2(d) show

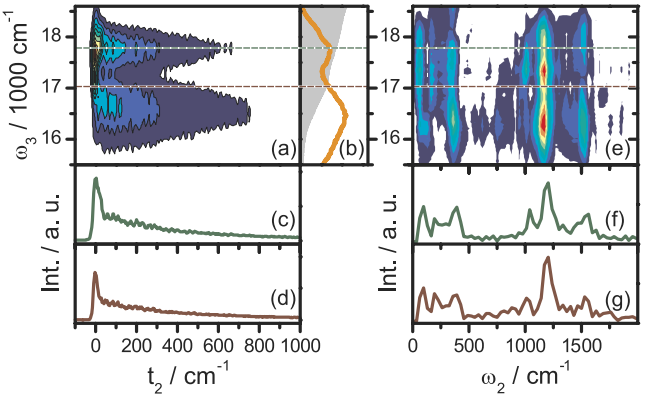

FIG. 2. (a) Detection frequency (ω_3) resolved transient grating signal of LH2 *M. pur.* (b) Absorption spectrum in gray in comparison to the spectrum of the excitation pulse in orange. Temporal cuts at S_2-specific detection frequencies specific for S_2 and Q_x in (c) and (d), respectively. (e) Fourier-transform spectra along t_2, dispersed along ω_3. (f) and (g) show cuts through (e) for S_2- and Q_x-specific detection frequencies, respectively.

the respective transients. For both detection frequencies, we observe a fast decaying peak around $t_2 = 0$ fs, followed by a slower mono-exponential decay with a decay constant of 330 ± 50 fs according to least square fit analysis. The signal does not decay to zero within the 1000 fs time window of the experiment. The observed decay behavior is, within error margins, identical for both detection frequencies. TG probes the sum of the absorptive and dispersive part of the induced third order signal, while pump-probe selects only the absorptive part, meaning that the retrieved time constants cannot be directly compared to pump-probe measurements.[48,49] Vibrational dynamics will however yield similar frequencies between the two techniques (see, e.g., vibrational dynamics in β-carotene investigated by pump-probe[18,50] and by TG[51,52]). The vibrational response manifests as an oscillatory signal, superimposed on a slowly varying background. After subtraction of the latter and Fourier transformation of the remaining signal along t_2 for every detection frequency, the (ω_2 , ω_3) frequency map in Fig. 2(e) is retrieved. A cut along a S_2-specific detection frequency (green dashed line) yields the well-known carotenoid frequencies as depicted in Fig. 2(f) near 1000 cm^{-1} (methyl-rocking motion), 1160 cm^{-1} (carbon single bond stretching), and 1530 cm^{-1} (carbon double bond stretching) and are in agreement with resonance Raman spectra measured for okenone.[53] The same set of frequencies is observed when detecting at the Q_x-band, as shown in Fig. 2(g). This is interesting because BChl-specific modes near 1600 cm^{-1} or 700 cm^{-1} as known from resonance Raman measurements[54] are not found. The absence of BChl vibrational signatures is readily explained by vibrational-electronic coupling in BChl, which is small in comparison to carotenoids.[16]

C. 2D electronic spectroscopy

As mentioned in Sec. II, 2D-ES and TG are related in the sense that they are both four wave mixing techniques. The difference lies in the treatment of the first inter-pulse delay t_1, which is kept at zero in TG, but scanned and Fourier-transformed ($t_1 \rightarrow \omega_1$) in 2D-ES. The emerging (ω_1, ω_3)-2D

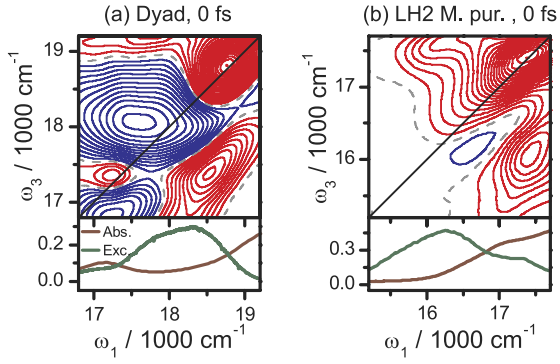

FIG. 3. 2D electronic spectra of the dyad (a) and LH2 *M. pur.*, each at $t_2 = 0$ fs. Positive (negative) signals are drawn as red (blue) full lines at 5% steps. Each figure is normalized to its respective maximum. The dashed grey lines mark the nodal line at zero intensity. The lower panels in each graph show the overlap between absorption (dark red line) and excitation spectrum (green line).

plots, recorded at a fixed second inter-pulse delay t_2, allow for a correlation of excitation (ω_1) and emission frequencies (ω_3). Fig. 3 compares electronic 2D spectra at $t_2 = 0$ fs for the dyad and LH2 *M. pur*.

At $t_2 = 0$ fs, electronic population is given no time to relax to lower lying states, within experimental time resolution. Both spectra in Fig. 3 show strong positive (red) peaks along the diagonal ($\omega_1 = \omega_3$). Comparison to the absorption spectra, given in the lower panels in Figs. 3(a) and 3(b), shows that the strong diagonal peaks stem from the carotenoid's $S_0 \rightarrow S_2$ transition. The dyad's spectrum in Fig. 3(a) shows two well resolved diagonal peaks corresponding to the Q_x-transition at approximately 17 200 cm^{-1} and a carotenoid peak near 19 000 cm^{-1}. We note that no sign of a diagonal peak between S_2- and Q_x-related features is detectable, speaking against the involvement of intermediate states such as S_x in this molecule.[7] The off-diagonal or cross peaks ($\omega_1 \neq \omega_3$) with negative amplitude in Fig. 3 stem from ESA-pathways. For carotenoids, ESA from S_2 in the visible has been observed.[15,17] The ESA of the dyad's porphyrinic acceptor was described previously as broad and featureless.[25] While the combination of donor and acceptor ESA explains the negative features in the dyad's 2D-spectrum, we note that at $t_2 = 0$ fs, negative signals do not necessarily have to be related to ESA, as they already occur in a two level system at this waiting time.[55] Positive off-diagonal peaks can stem from vibrational energy levels,[28,56–58] SE or coupling between two electronic transitions.[55] The latter would be the most interesting scenario, as electronic coupling between donor and acceptor would suggest an excitonic energy level structure and the associated transfer mechanisms.[59] Upon visual inspection, the location of the positive cross peaks in the dyad's 2D signal suggests electronic coupling as a likely explanation. The stronger of the two positive cross peaks, found below the diagonal ($\omega_1 > \omega_3$), peaks at a value of ω_3 that coincides with the absorption frequency of the Q_x-band. There is also a corresponding peak above the diagonal ($\omega_1 < \omega_3$), which peaks blue detuned with respect to Q_x and with weaker intensity than its counterpart below the diagonal. Such differences in intensity may however be attributed to the ultrafast population transfer from S_2 to Q_x, the onset of which takes place within the experimental time resolution of 11 fs. The blue detuned maximum of the upper cross peak can be attributed to finite pulse width or effects of chirp in the excitation pulses.[60] Inspection of the 2D signal of LH2 *M. pur.* disproves the assumption of electronic coupling. The major difference between the dyad and LH2 *M. pur.* is the position of the S_2-transition. While the dyad's carotenoid exhibits maximum absorption above 19 000 cm^{-1}, the carotenoid in LH2 *M. pur.*, okenone, has a carbonyl-containing endgroup as shown in Fig. 1(d), shifting the 0-0 transition of okenone *in vivo* down to 17 570 cm^{-1},[61] while the energetic position of the Q_x-band remains unchanged between dyad and LH2 *M. pur*. Hence, the energy difference between S_2 and Q_x should be greatly reduced in LH2 *M. pur.*, and the corresponding cross peaks should be shifted, leading to a large and fairly featureless electronic 2D-signal. In contrast to this expectation and in comparison to the dyad in Fig. 3(a), the lower cross peak in LH2 *M. pur.* shows roughly the same energy difference from the diagonal of approximately 1500 cm^{-1}. This strongly suggests a vibrational origin, given that the prominent C=C stretching mode of carotenoids is found at this energy.

The peak above the diagonal in LH2 *M. pur.* is harder to explain. The ESA-signal in Fig. 3(b) is much weaker than for the dyad, which is readily explained by a different ESA-transition energy from S_2 for okenone *in vivo*.[48] We can thus observe a weak diagonal peak at $\omega_1 = \omega_3 \approx 16\,480$ cm^{-1}, with an excitation frequency ω_1 corresponding to the upper cross peak. This energetic position excludes coupling to Q_x, peaking at 17 035 cm^{-1}, as a possible explanation in LH2 *M. pur*. The physical origin of the upper cross peak in Fig. 3(b) becomes more obvious when examining the peak shape evolution along t_2, as shown in Fig. 4.

The upper cross peak at ($\omega_1 = -16\,000$ cm^{-1}, $\omega_3 = 17\,500$ cm^{-1}) is discernible up to 30 fs, but drops to zero by 80 fs. This behavior is unexpected for an electronic coupling peak. The rapid decay of the upper cross peak rather suggests that it is an artifact, related to the shape of the excitation pulses. The excitation spectra are clearly non-Gaussian (see lower panel of Fig. 3(b)), making limited pulse width or chirp related effects[60] the most likely explanation for the upper diagonal cross peak for LH2 *M. pur*.

Another interesting feature is observed at $\omega_1 = -17\,500$ cm^{-1} and $\omega_3 = 16\,480$ cm^{-1}, i.e., an energetic position indicative of $S_2 \rightarrow Q_x$ energy transfer pathways. The peak builds up rapidly within the first 30 fs, which corresponds well with the 55 fs transfer time reported for this process.[48] After 50 fs, negative ESA-signals dominate the spectra. This is explained by the intramolecular $S_2 \rightarrow S_1$ energy transfer, occurring at a 95 fs build up rate as reported previously.[48] We support this assignment by calculating the electronic 2D-spectra only for okenone, the carotenoid of LH2 *M. pur*. Details of the calculations can be found in Sec. II C.

IV. DISCUSSION

A. Carotenoid-chlorophyll interaction

Spectroscopic experiments reveal the transfer from carotenoid S_2 and S_1 states to Chls and BChls as fast and relatively efficient despite the rather short S_2 state life time of

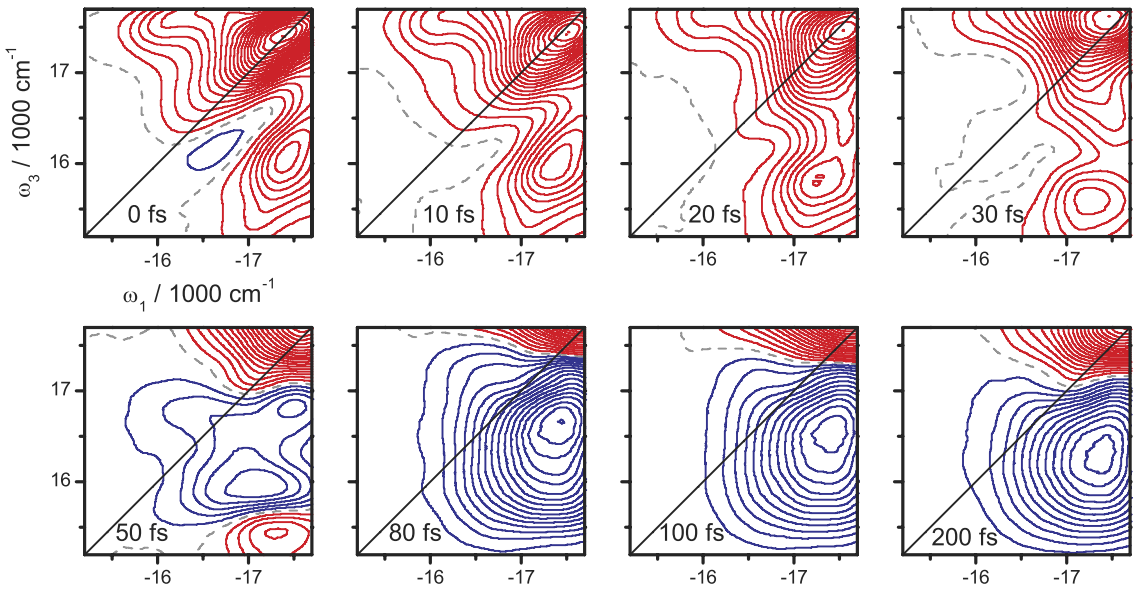

FIG. 4. Electronic 2D spectra of LH2 *M. pur.*, measured at indicated values of t_2. Line coloring follows the same conventions as described in Fig. 3.

the monomeric carotenoid (at least in comparison with Chls and BChls). Both Q_x and S_2 states are optically allowed, and they can therefore interact by resonance coupling mechanism. Because of the proximity of the two molecules in the LH2 structure, one cannot exclude an electron exchange (Dexter) mechanism. However, quantum chemical calculations suggest Coulomb interaction to be dominant here.[62] In this case, the theoretical description, the carotenoid-BChl interaction, and modeling of the corresponding excitation energy dynamics remain within the well understood framework of excitonic description of photosynthetic antennae.[59,63]

In the standard framework, we assume the electronic coupling element between the two electronic states to be independent of the vibrational degrees of freedom (DOF) of the molecular system. Electronic excitation is transferred between the two molecules due to an interplay of the resonance coupling and the fast fluctuations of the molecules' respective energy gaps. The energy gap fluctuations are caused by their interaction with the nuclear DOF which involve both the intra- as well as intermolecular vibrations. These are considered a thermodynamic heat bath characterized by a certain temperature and spectral density. Two regimes of the relative coupling strengths are usually distinguished. The *delocalized regime* in which the system-bath interaction is weak in comparison with the resonance interaction between the molecules, and the *localized regime* in which the system-bath coupling is considered strong. The terms localized and delocalized refer to the effective electronic eigenstates of the interacting system. For the delocalized regime, the coupling between the two molecules is strong enough to sustain correlation between the electronic excitations on different molecules so that delocalized excitons are formed. In the localized regime (also referred to as Förster regime here), the system-bath interactions induce energy gap fluctuations which prevent any such correlation, and the excitations appear to be localized on the molecules. In fact, even in relatively weakly excitonically coupled systems, one can often detect signs of delocalization (see, e.g., Ref. 64), because the actual apparent eigenstates are always somewhere in between the two theoretical limits. For photosynthetic aggregates formed by BChl and Chl molecules, where the protein bath can be to some extent assumed as unstructured, modern simulation methods such as the Hierarchical Equations of Motion (HEOM) enable us to determine the excited state dynamics beyond the two limits mentioned above.[65] However, even in the case of aggregates composed of BChl or Chl molecules only, some clearly visible spectroscopic features can result from the involvement of pronounced vibrational modes.[66–69]

In the discussion that follows, we want to argue that the involvement of the vibrational DOF of the carotenoid molecules is crucial for the energy transfer dynamics between the S_2 and the Q_x states. We will compare two theoretical approaches to the calculation of the energy transfer rates, both motivated by the observed features of the spectra and known spectroscopic behavior of the system. We will argue that both support the crucial role of the fast vibrational modes, in particular, the carotenoid ground state vibration levels.

The Hamiltonian of the relevant part of the system (state Q_x of the BChl and the S_2 state of the carotenoid) can be written in the following way:

$$\begin{aligned} H = {} & H_{Q_x}^{(B)} + H_{S_2}^{(B)} + \left(\epsilon_{Q_x} + \Delta V_{Q_x}(q^{(Q_x)})\right) |Q_x\rangle\langle Q_x| \\ & + \left(\epsilon_{S_2} + \Delta V_{S_2}(q^{(S_2)})\right) |S_2\rangle\langle S_2| \\ & + J\left(|S_2\rangle\langle Q_x| + |Q_x\rangle\langle S_2|\right). \end{aligned} \tag{8}$$

Here, ϵ_{Q_x} and ϵ_{S_2} are the optical electronic transition energies of the BChl Q_x state and the carotenoid S_2 state, respectively (including the reorganization energy of the bath), $H_{Q_x}^{(B)}$ and $H_{S_2}^{(B)}$ are the Hamiltonian operators of the nuclear DOF on the BChl and carotenoid, respectively. These two sets of nuclear DOF described by macroscopic coordinates $q^{(Q_x)} = \{q_1^{BChl}, \ldots, q_n^{BChl}\}$ and $q^{(S_2)} = \{q_1^{Car}, \ldots, q_n^{Car}\}$, where n is a macroscopically large number, form the bath interacting through operators $\Delta V_{Q_x}(q^{(Q_x)})$ and $\Delta V_{S_2}(q^{(S_2)})$ with the electronic transitions on the BChl and carotenoid,

respectively. The electronic coupling element J describes the resonance interaction between the collective excited state $|Q_x\rangle = |e_{Q_x}\rangle|g_{Car}\rangle$ in which the BChl is excited to the state Q_x and the carotenoid is in its electronic ground state and the collective excited state $|S_2\rangle = |g_{BChl}\rangle|e_{S_2}\rangle$ in which the BChl is in its electronic ground state and the carotenoid is excited to its excited state S_2. To complete the Hamiltonian, we should also to include the state $|f\rangle = |e_{Q_x}\rangle|e_{S_2}\rangle$ in which both Car and BChl are excited. However, it will be shown later that the features related to this state are negligible as the resonance coupling will be shown to be weak. In the experimental 2D spectra, shown in Fig. 4, one can easily identify the fast rising ESA component, which is usually assigned to the strong absorption from the S_1 states of the carotenoid. Contribution of this state is taken into account by including a separate partial Hamiltonian and $S_2 \rightarrow S_1$ relaxation rate into the response functions in the Appendix . All other states with no spectroscopic contributions are taken into account in the simulations by introducing decay rates for the bright states. For the subsequent discussion, it will be useful to introduce a bare electronic (single exciton) Hamiltonian which reads as

$$H_{\mathrm{el}} = \epsilon_{Q_x}|Q_x\rangle\langle Q_x| + \epsilon_{S_2}|S_2\rangle\langle S_2| + J\left(|S_2\rangle\langle Q_x| + |Q_x\rangle\langle S_2|\right). \quad (9)$$

This Hamiltonian represents the basic three level (ground state energy was chosen to be zero) structure of the problem.

B. Energy transfer rates

As discussed above, the interplay of energy gap fluctuations and the resonance coupling energy determines which theoretical limit applies. The usual discussion of the relative strengths of the two interactions is made based on the relative values of the reorganization energy λ which describes the magnitude of the energy gap fluctuations and the value of the resonance coupling J.[70] Our system is characterized by reorganization energies λ_{Q_x} of the BChl and λ_{S_2} of the Car which should be compared to the resonance coupling energy J. For the validity of the weak resonance coupling limit, it is usually required that $\lambda > |J|$. In our case, assuming $J \approx 100\ \mathrm{cm}^{-1}$ (see Refs. 38 and 71) confirms the validity of this regime because the total λ_{S_2} is in the order of thousands of cm^{-1} as it involves two fast vibrational modes with HR-factors close to 1 and vibrational frequencies above $1000\ \mathrm{cm}^{-1}$ as shown in Fig. 2. The Q_y state of BChl in the protein environment of the LH2 complex exhibits $\lambda_{Q_y} \approx 100\ \mathrm{cm}^{-1}$ (see, e.g., Ref. 72) and we can assume a similar value $\lambda_{Q_x} \approx 100\ \mathrm{cm}^{-1}$ as for the Q_x state. Here, the reorganization energy of the chromophore is only comparable, not larger, than the resonance coupling element. We note that conventionally, the role of temperature is completely neglected in this discussion. The magnitude of the energy gap correlation function, which provides a true measure of the energy gap fluctuations, depends on temperature and the dependency is linear in the high temperature limit (in the case of Brownian oscillator model, see Ref. 73). It would therefore be more suitable to compare the value of $\lambda k_B T$ and $|J|^2$. At room temperature, $k_B T = 207\ \mathrm{cm}^{-1}$ and $\lambda_{Q_x} k_B T > |J|^2$. Yet another problem arises when considering the role of the relative energy gap $\Delta\varepsilon = \epsilon_{S_2} - \epsilon_{Q_x}$ of the Q_x and S_2 states. In an ideal dimer, the delocalization is determined by the so-called mixing angle $\theta = \frac{1}{2}\arctan\frac{2|J|}{|\Delta\epsilon|}$.[74] The delocalization decreases with the increasing $\Delta\varepsilon$. The interplay of the relative energy gap, temperature, reorganization energy, and resonance energy is a subject of numerous theoretical studies in the context of photosynthesis. However, no simple formula taking into account the influences of all these parameters on the degree of delocalization exists.

After the discussion of the parameters of the carotenoid-BChl dimer, we have many reasons to believe that the interaction of the S_2 and Q_x states can be treated in the weak coupling limit. The issues are however more complicated because of the nature of the system-bath interaction in the carotenoid. Most of its reorganization energy can be assigned to the fast intramolecular vibrational modes. The spacing between the vibrational levels and the relative electronic energy gap $\Delta\varepsilon$ are such that the Q_x state can be viewed as effectively interacting with the nearest vibrational levels and not with the carotenoid electronic state as a whole. This is a situation similar to the one studied in Refs. 66, 68, and 69 where special resonances between vibrational and electronic energy gaps lead to pronounced effects despite the small HR-factors of the BChls. Clearly, treating the carotenoid vibrations as a thermodynamic bath is a questionable approximation.

In Subsections IV B 1 and IV B 2, we will briefly discuss the carotenoid-BChl energy transfer rates based on the weak coupling Förster theory and compare it with an explicit treatment of the carotenoid vibrations in the Hamiltonian, along with Refs. 66 and 69. The energy level structure characteristic for the two situations is presented in Fig. 5.

1. Weak resonance coupling limit

In the weak resonance coupling limit, the parameter J of the Hamiltonian, Eq. (8), is assumed small and perturbation theory to the second order can be performed. For two transitions (donor and acceptor), the transition rate is given by the Fermi golden rule as $K_{A\leftarrow D} = \frac{2\pi}{\hbar}|J|^2\delta(\epsilon_D - \epsilon_A)$. It is possible to view the donor molecule as a set of many available de-excitation transition (the molecule is excited electronically and vibrationally) while the acceptor molecule can be viewed as a set of transitions ready to be excited. In a realistic case, it is therefore necessary to integrate the Fermi formula over all acceptor and donor transitions

$$K_{A\leftarrow D} = \frac{2\pi}{\hbar}|J|^2\int_{-\infty}^{\infty}\mathrm{d}\epsilon_D\int_{-\infty}^{\infty}\mathrm{d}\epsilon_A f_{\mathrm{abs}}(\epsilon_A) f_{\mathrm{fl}}(\epsilon_D)\delta(\epsilon_D - \epsilon_A), \quad (10)$$

where f_{abs} and f_{fl} correspond to the normalized distribution of the transition energies available for excitation on the acceptor and the normalized distribution of the transition energies available for the de-excitation on the donor. The Förster rate can be derived directly from Eq. (10) by noticing that the acceptor absorption spectrum is related to the distribution of transition frequencies $\tilde{f}_{\mathrm{abs}}(\omega) = f_{\mathrm{abs}}(\hbar\omega)$ as $\alpha(\omega) \sim \omega\tilde{f}_{\mathrm{abs}}(\omega)$ and similarly for the donor fluorescence spectrum $\sigma(\omega) \sim \omega^3\tilde{f}_{\mathrm{fl}}(\omega)$ (see, e.g., Refs. 63 and 74) or directly by perturbation theory

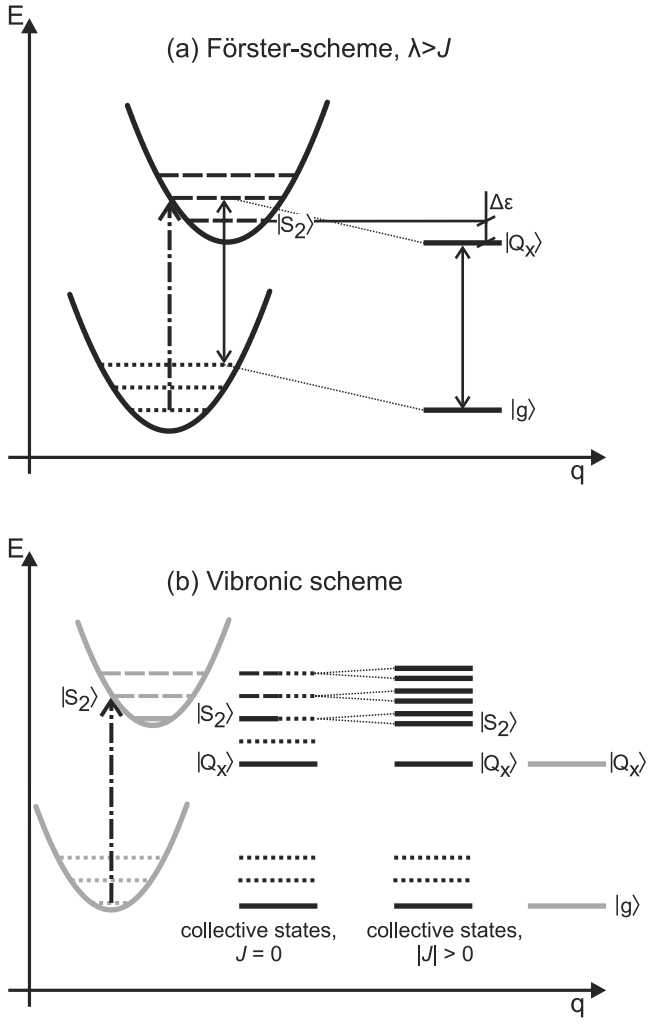

FIG. 5. Interaction schemes of the electronic and vibrational levels in (a) localized (Förster) and (b) delocalized (vibronic) regime. In the case (a), the transition energy from the non-equilibrated state of the carotenoid excited state vibrations has to be resonant with the Q_x transition energy. The relative energy gap $\Delta\varepsilon$ between the S_2 and Q_x transitions requires involvement of more than one vibrational quanta of the carotenoid. The vibronic case (b) also involves excitonic mixing of the vibrational levels of the carotenoid with the Q_x transition. The collective single excited states of the carotenoid-purpurin or carotenoid-BChl dimer involve states in which the electronic Q_x transition and vibrational modes on the electronic ground state of the carotenoid are excited simultaneously. The states can excitonically mix with the carotenoid electronically excited state with a different number of vibrational quanta.

with respect to J and a cumulant expansion for the bath DOF as in Ref. 59. In both cases, there is a direct relation between the rate and the overlap of absorption spectrum of the acceptor with the emission spectrum of the donor

$$K_{A\leftarrow D} = 2\pi \frac{|J|^2}{\hbar^2} \frac{\int d\omega \alpha_A(\omega)\sigma_D(\omega)\omega^{-4}}{\int d\omega \alpha_A(\omega)\omega^{-1} \int d\omega \sigma_D(\omega)\omega^{-3}}. \quad (11)$$

It is important to note that Förster theory does not, in general, depend on the dipole-dipole coupling approximation although the specific dependence of the rate in this approximation is often used. For the scope of the present manuscript, the coupling energy J can be calculated by any type of advanced methods of quantum chemistry which takes into account all the details of the electronic structure of the excited states of the interacting molecules.[75] From the theoretical point of view, the Förster rate can be derived from Hamiltonian, Eq. (8), under various assumptions. Usually, one assumes relaxed state of the environment and the intramolecular vibrational modes. However, Förster theory is very versatile and allows many generalizations;[75,76] most importantly, it is still valid for the case that the excited state of the donor is unrelaxed.[73] Equation (10) is then still valid, but it does not result in Eq. (11). Förster theory, therefore, also allows for a direct experimental estimation of the resonance coupling if the fluorescence spectrum of the donor and the absorption spectrum of the acceptor are known, even in case that the fluorescence does not start from a relaxed state. For the present dyad,[24] the coupling J was determined to be $J = 240\ \mathrm{cm}^{-1}$, within the framework of Eq. (11).

Fig. 5(a) describes a typical situation for the short time dynamics of the $S_2 \rightarrow Q_x$ energy transfer. The higher vibrationally excited levels of S_2 are populated, and in order to achieve resonance with the Q_x transition, even higher vibrational levels on the carotenoid ground state S_0 are excited after de-excitation of the donor (S_2). The energy transfer is enabled by the fact that the energy corresponding to the $\Delta\varepsilon$ is accepted by the ground state vibrational levels of the carotenoid molecule as depicted in Fig. 5(a). The same statement can be rephrased in terms of the spectral overlap. Because the rate depends on the overlap of the donor emission and the acceptor absorption spectra, the effective broadening of the carotenoid fluorescence spectrum due to the fast vibrational modes increases significantly the energy transfer rate. Förster theory thus assigns the electronic ground state vibrational levels of the carotenoid a crucial importance in the energy transfer process between electronically excited states.

2. Vibronic coupling

The main conclusion of Sec. IV B 1 is that the high frequency vibrational modes of the carotenoid are an important driving element of the energy transfer from S_2 to Q_x. Förster theory shows that these modes provide resonance for energy transfer and that this resonance involves multiple vibrational quanta. As one can learn from Fig. 1(a), upon coupling, the absorption lineshape undergoes a slight change in the carotenoid region suggesting weak delocalization between Q_x and S_2 states, at least for the dyad. It is, therefore, natural to include the primary vibrational mode of the carotenoid (see Sec. II C 2) explicitly into the Hamiltonian, and to treat only the remaining secondary overdamped modes as a bath. This leads directly to the model of vibronic excitons (see Refs. 66–68 and 77). Such a model automatically treats the primary vibrational modes non-perturbatively.

We split the nuclear part of the carotenoid Hamiltonian in Eq. (8) into the primary mode denoted by coordinate $\tilde{q}$ and the rest of the modes (secondary modes) which we denote by $q'^{(S_2)}$ (see Sec. IV A for the notation). We have

$$H_{S_2}^{(B)} = H_{S_2}^{(b)} + H_{\mathrm{vib}} + H_{\mathrm{vib-b}}, \quad (12)$$

where $H_{S_2}^{(b)}$ is the Hamiltonian of the secondary bath and the Hamiltonian of the primary mode and its interaction with the

secondary bath read as

$$H_{\mathrm{vib}} = \frac{\hbar\tilde{\omega}}{2}\left(\tilde{p}^2 + \tilde{q}^2\right) \tag{13}$$

and

$$H_{\mathrm{vib-b}} = -\tilde{q}\sum_k \xi_k q_k. \tag{14}$$

Here, $\tilde{\omega}$ is the frequency of the primary mode to be treated explicitly, and q_k are the coordinates from the set $q'^{(S_2)}$ coupled to the primary mode by a coupling constant ξ_k. In the excited state of the carotenoid, the bath Hamiltonian is now split in the following way:

$$H_{S_2}^{(B)} + \Delta V_{S_2}(q^{(S_2)}) = H_{S_2}^{(b)} + \Delta V_{S_2}(q'^{(S_2)}) + \frac{\hbar\tilde{\omega}}{2}\left(\tilde{p}^2 + (\tilde{q}-d)^2\right) - (\tilde{q}-d)\sum_k \xi_k q_k. \tag{15}$$

Here, we assume that the same secondary bath which drives the ground state vibrations into the equilibrium drives also the excited state vibrations to their corresponding equilibrium. Correspondingly, the energy gap operator reads as

$$\Delta V_{S_2}(q^{(S_2)}) = \Delta V_{S_2}(q'^{(S_2)}) - \hbar\tilde{\omega}d\tilde{q} + d\sum_k \xi_k q_k. \tag{16}$$

The energy gap operator, Eq. (16), is composed of three parts, $\Delta V_{S_2}(q'^{(S_2)})$ representing the overdamped bath, the part representing the direct influence of the primary mode on the energy gap fluctuations

$$H_{\mathrm{el-vib}} = \hbar\tilde{\omega}d\tilde{q}, \tag{17}$$

and the part describing the influence of the overdamped bath on the electronic energy gap functions via coupling with the primary mode. The strength of the latter part of the interaction Hamiltonian is given by the shift d of the excited state vibrational potential with respect to the ground state potential. The essence of the vibronic model is to include $H_{\mathrm{el-vib}}$ to the Hamiltonian which we treat explicitly. Only an effective energy gap operator

$$\Delta V_{S_2}^{(\mathrm{eff})}(q'^{(S_2)}) = \Delta V_{S_2}(q'^{(S_2)}) + d\sum_k \xi_k q_k \tag{18}$$

is treated by perturbation theory. It leads to the bath correlation function

$$C(t) = \langle \Delta V_{S_2}(q'^{(S_2)};t)\Delta V_{S_2}(q'^{(S_2)};0)\rangle + C_{\mathrm{b}}^{(\mathrm{el})}(t), \tag{19}$$

where the last term on the right hand side corresponds to the direct contribution of the secondary bath to the dephasing. The damping of the primary mode is governed by the bath correlation function originating from the term, Eq. (14),

$$C_{\mathrm{b}}(t) = \sum_k |\xi_k|^2\langle q_k(t)q_k\rangle, \tag{20}$$

while the direct contribution of the secondary bath to the dephasing is expressed by the same correlation function scaled by the dimensionless shift of the effective vibrational mode

$$C_{\mathrm{b}}^{(\mathrm{el})}(t) = |d|^2 C_{\mathrm{b}}(t). \tag{21}$$

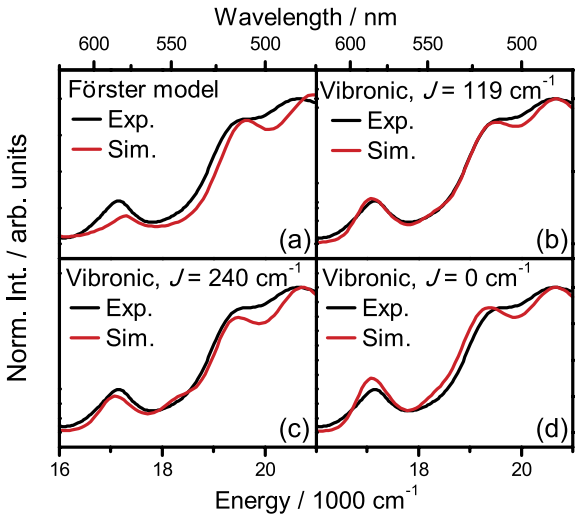

FIG. 6. Absorption spectra of the dyad. Panel (a) shows the sum of the monomeric spectra, which corresponds to the weak coupling case (no changes to the lineshape except of lifetime broadening); (b) presents the best fit of the dyad spectrum with the Q_x transition energy, relative energy gap $\Delta\varepsilon$, carotenoid HR factors, and the resonance coupling free to be adjusted. Panel (c) shows the best fit with the resonance coupling fixed at $J = 240\ \mathrm{cm}^{-1}$ and panel (d) presents the sum of the monomers with the parameters corresponding to the best fit from panel (b), but with $J = 0\ \mathrm{cm}^{-1}$.

The calculation of the energy transfer dynamics in the vibronic model thus starts with a diagonalization of the Hamiltonian

$$H_S = H_{\mathrm{vib}} + H_{\mathrm{el-vib}}|S_2\rangle\langle S_2| + H_{\mathrm{el}}. \tag{22}$$

The diagonalization results in vibronic eigenstates which mix the electronic and vibrational states. In a second step, the rates of population transfer and coherence dephasing are calculated for the set of eigenstates by second order perturbation theory cumulants.[39] Correlation function, Eq. (20), was used to describe damping of the primary mode. The electronic dephasing described by correlation function, Eq. (19), was assumed to be dominated by the secondary bath contribution $C_{\mathrm{b}}^{(\mathrm{el})}(t)$. This choice decreases the number of degrees of freedom in fitting and effectively ties the strength of the coupling between the primary mode and the secondary bath to the strengths of the interaction between the electronic transition and the primary mode. Because only the effective spectral density is important for the calculation of transition rates, we believe that the advantage in limiting the number of parameters outweighs the restriction put on our model. In principle, one could estimate the overall rate of energy transfer directly by weighting the calculated rates between individual levels. We have, however, chosen the more practical approach of calculating the transfer time as described in Sec. II C 2.

Because of the rather large vibrational frequency and moderate coupling, the Q_x transition can be viewed as interacting only with the energetically nearest transition. This situation is depicted in Fig. 5(b). For the sake of clarity of the graphical presentation, we depict a situation of perfect resonance between the relative energy gap $\Delta\varepsilon$ and the vibrational frequency and show energy level splitting of the energetically nearest levels. Fig. 5(b) depicts the relevant carotenoid and BChl energy levels as two separate entities (in gray) and in terms of

collective states of the carotenoid-BChl dimer in the case of $J = 0$. Conceptually, the ground state vibrational levels of the carotenoid contribute to an excited collective state if the Q_x state is excited. This is a consequence of the fact that in a singly excited aggregate state, all molecules except one (carotenoid) are in their ground state. The ground state vibrational levels of the carotenoid thus interact resonantly with the vibrational levels of the carotenoid in the electronically excited state S_2. This interaction corresponds to the energy transfer from S_2 to Q_x with a simultaneous deposition of the excess energy to the ground state vibrations of the carotenoid. The complete picture of the energy levels of the system is much more complicated because the excitonic mixing involves all available states. The details of this mixing, which are included in the basis transformation from the localized states to the energetic eigenstates, lead to discernible changes in the lineshape of the carotenoid molecule. As will be demonstrated in Secs. IV C and IV D, the vibronic model provides an explanation for the observed spectral changes as shown in Fig. 1(a). Also, the detailed treatment of the interaction between carotenoid vibrational levels and the Q_x state leads to the experimentally observed energy transfer rates with a significantly weaker resonance coupling than predicted by Eq. (11).

C. Simulation of absorption spectra and transfer rates in vibronic model

The vibronic model discussed in Sec. IV B was implemented as described in Sec. II C 2. The absorption spectra of monomeric carotenoid were fitted with a model Hamiltonian involving one effective high frequency primary mode to obtain starting values of the effective mode parameters for the subsequent fitting of the absorption spectra of the dyad and the LH2 complex. We found the frequency of the vibrational mode in the dyad to be $\omega_{\text{eff}} = 1390\ \text{cm}^{-1}$ and its HR-factor was determined to be $s_{\text{eff}} = 1.3$. All monomeric parameters are discussed in Sec. II C 2.

In Fig. 6, we summarize our fitting efforts for the dyad. We chose the dyad because the same solvent can be used for the dyad and its components avoiding solvent related bathochromic shifts. The absorption spectra of LH2 *M. pur.* and LH2 *Rps. ac.* were equally well reproduced with the employed vibronic model. Fig. 6(a) presents the result of summation of the dyad's monomer spectra. This is the spectrum corresponding to the weak resonance coupling case (Förster regime) and it is presented to highlight the changes between monomeric and dyad spectra. In Fig. 6(b), we present a result of the fitting in which the HR-factor of the carotenoid, the Q_x transition frequency, the relative energy gap $\Delta\varepsilon$ between S_2 and Q_x, and the resonance coupling J were allowed to change. The fitting achieves good agreement with the experimental dyad spectrum, most importantly in the carotenoid related part. There the relative height of the absorption maxima of different vibrational peaks changes between the monomer and the dyad. The estimated coupling is $J = -119\ \text{cm}^{-1}$ while $s_{\text{eff}} = 1.29$, $\Delta\varepsilon = 2400\ \text{cm}^{-1}$, and $\epsilon_{Q_x} = 17\,150\ \text{cm}^{-1}$. The minor change with respect to the parameters of the monomers, such as the change of the transition energy to the excited state, has to be assigned to the chemical change upon formation of the dyad.[24]

The same fitting procedure with fixed resonance coupling J estimated from measured fluorescence spectrum by Förster theory, $J = 240\ \text{cm}^{-1}$,[24] results in a less satisfactory agreement as can be seen in Fig. 6(c). In order to demonstrate that lineshape changes in all cases are not only due to the change of the monomeric HR-factor of the carotenoid molecule, we show the absorption spectrum of the dyad with optimized parameters after setting $J = 0\ \text{cm}^{-1}$ in Fig. 6(d). Interestingly, the best fit is achieved with a change of the HR-factor of less than 1% and the change in the line shape can be therefore mostly assigned to the resonance coupling.

The simulation of the absorption spectrum has resulted in a value of J which is by 50% smaller than the one estimated from the experiment, suggesting that higher value is not compatible with the spectral changes with respect to the monomers seen in the dyad. The obvious question is whether this lower value for the resonance coupling is compatible with the measured ultrafast rates. To this end, we perform calculations of the S_2 to Q_x transfer dynamics to estimate the transfer time introduced in Sec. II C 2 for various values of J and $\Delta\varepsilon$ and keeping other parameters of the model fixed to those from the best fit from Fig. 6(b). The plot of transfer time as a function of J and $\Delta\varepsilon$ is presented in Fig. 7. The calculations yield a transfer time of $\tau_{S_2\to Q_x} = 55$ fs for the values of the best fit which is in good agreement with the experimental value of 40 fs.[24] Moreover, the 2D plot in Fig. 7 and the corresponding cut at the value of $J = -119\ \text{cm}^{-1}$ reveal a periodic modulation of the transfer time with the period corresponding to the effective spacing between vibrational levels. The transfer time decreases monotonically with increasing value of J, as shown in the lower panes of Fig. 7 representing cuts along the experimental values of $\Delta\varepsilon$. The periodic modulation of the transfer time is in agreement with the resonant involvement of carotenoid vibrational modes in energy transfer. As in the Förster case, this implies the involvement of the carotenoid vibrational levels from the electronic ground state. Conservation of energy during the energy transfer requires the excess energy to be deposited to the vibrational energy of the carotenoid.

D. Simulation of the 2D spectra

In order to assign the observed features of the experiment 2D-spectrum, we performed simulations of the carotenoid 2D spectra. This is a first step towards a complete simulation of the interacting Car-BChl system, which allows us to assign Car only features and possibly identify 2D spectral components originating in Q_x state. Such a full calculation will be a subject of our future work.

Calculating the 2D signal in a spectral region covering the edge of the studied molecule is an extremely difficult task given the fact that a good fit on the outer region of (even the absorption) spectrum depends on many rarely studied details of the chromophore interaction with its environment. For instance, assumptions about the Gaussian disorder of the electronic transitions energies and typical estimates for bath spectral densities are well suited for explaining the features around the maximum of absorption and do not cover well the situation at the edges of the spectra. On the other hand, introducing more fitting freedom by assuming arbitrarily some other types

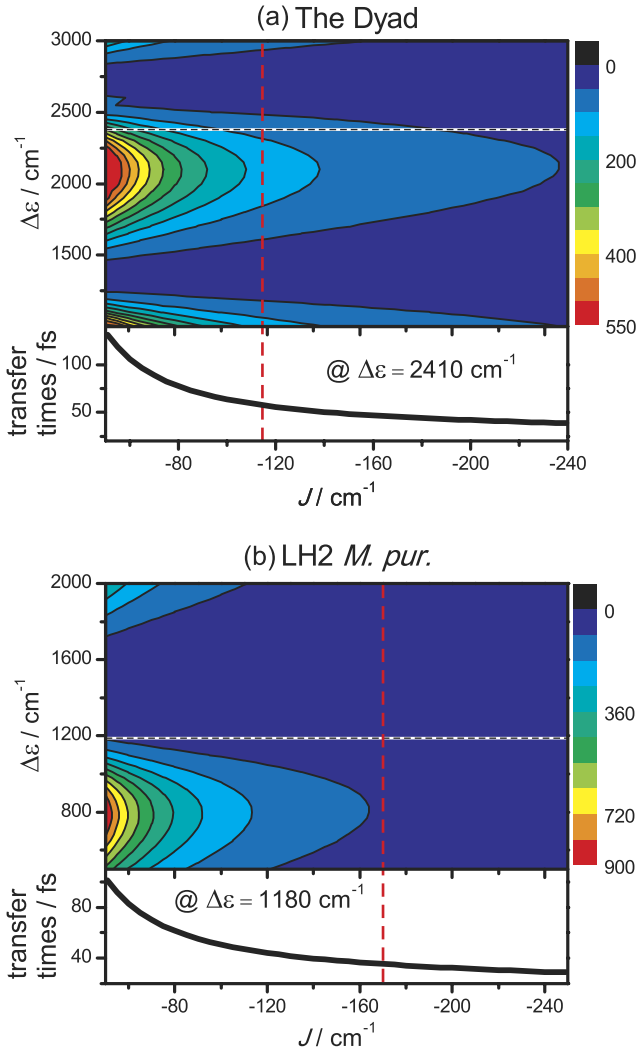

FIG. 7. Transfer time as a function of J and $\Delta\varepsilon$ for the dyad (a) and for LH2 *M. pur.* (b). At the experimental value of $\Delta\varepsilon$ and the values of resonance coupling determined by fitting the absorption spectrum, transfer time for the dyad and LH2 *M. pur.* are 55 fs and 40 fs, respectively, in agreement with the values reported in pump probe measurements.

of spectral densities and disorder distributions seems not to yield more theoretical insight, as the new parameters cannot be fixed by a limited set of experiments. Below, we therefore describe a calculation of the carotenoid 2D-spectra in which the carotenoid molecule should well represent the carotenoid component of LH2 *M. pur*. Correspondingly, a limited fitting to the experiment 2D-spectra from Fig. 4 is done, keeping in mind that the two systems which are compared in such a fitting are different. Several carotenoid parameters are therefore taken from the literature.

1. Carotenoid only spectra

From the linear absorption spectrum of the LH2 complex, the electronic excitation energy $\omega_{S_2S_0} = 19\,770$ cm^{-1} was obtained (see Fig. 1). Because of the line shape function approach, which relies on second-order cumulant expansion with the electronic ground state as the reference state, this value corresponds to the vertical transition energy, i.e., the sum of the electronic excitation energy and the reorganization energies of the spectral density components. The transfer rates $1/k_{S_2\rightarrow S_1} = 95$ fs and $1/k_{S_2\rightarrow Q_x} = 55$ fs were chosen in agreement with Ref. 48. Because of the slow transfer from S_1 to other electronic states, the lifetime broadening constant Γ_{S_1} was taken as zero. Although some spectral density parameters for okenone are available from the literature,[48] the respective parameters for β-carotene have been reported in more detail. They can provide some orientation for the choice of the parameters to model the okenone component of the investigated LH2 complex. According to Ref. 78, the frequencies of the included vibrational modes are $\omega_{UO,1} = 1150$ cm^{-1} and $\omega_{UO,2} = 1520$ cm^{-1}. The HR-factors of the vibrational modes in S_2 were assumed as $\chi_{UO,S_2S_2,1} = 0.25$ and $\chi_{UO,S_2S_2,2} = 0.5$. While these values are somewhat smaller than the ones for β-carotene given in Ref. 78, their ratio is similar. According to the tendency reported in the literature, the HR-factors in S_1 were assumed to be larger than those in S_2 by a scaling factor of 1.5. To describe the damping of the vibrational modes in S_1 with a time constant of 50 fs, ten Matsubara terms were taken into account in the calculation of the lineshape function. For one of the Brownian oscillator spectral density components, a fast decay with damping constant $1/\Lambda_{BO1,S_2S_2} = 30$ fs and a reorganization energy $\lambda_{BO,S_2S_2,1} = 300$ cm^{-1} in agreement with Ref. 79 was assumed. To reproduce the inhomogeneous broadening effects in the absorption spectrum of the LH2 complex, the second Brownian oscillator spectral density component with very slow decay constant of 20 ps[79] was included in the model. For a reorganization energy of $\lambda_{BO,S_2S_2,2} = 3000$ cm^{-1}, comparable inhomogeneous broadening effects as in a measured linear absorption spectrum could be obtained and features in the measured 2D-spectra could be qualitatively reproduced. In Ref. 80, it has been reported that coherence gets lost during this population transfer process, so that the fluctuations in S_2 and S_1 can be considered as uncorrelated. Accordingly, lineshape functions of the type $g_{S_2S_1}$ and $g_{S_2S_n}$ were taken as zero. The HR-factors for excitation from S_1 to S_n are known to be much smaller than the ones of the excitation from S_0 to S_2. In Ref. 48, a value of 0.1 is given, which was assumed for both modes in our calculation.

According to our interpretation, this value of the HR-factor is given with respect to S_0, as the vibrational energy for the transition between S_1 and S_n reported in Ref. 48 cannot be explained by such a small HR-factor. However, the much larger HR-factors of S_1 with respect to S_0 allow for a larger vibrational energy than expected from the value of 0.1 for the HR-factor.

Regarding the Brownian oscillator modes, it has been reported in Ref. 79 that for double excitation from S_1, the reorganization energy corresponds to a fraction of only 0.5 of the corresponding reorganization energy in S_1 from the electronic ground state, which was taken as the same as for S_2 in our description.

The vertical transition energy between S_1 and S_n was chosen as $\omega_{S_1S_n} = 15\,400$ cm^{-1} in agreement with Ref. 48. In the prefactors of the ESA response functions $\left|\frac{\mu_{S_1S_n}}{\mu_{S_0S_2}}\right|^2 = 1.5$ entered, following the values given in Ref. 81 for other carotenoid derivatives. The finite pulse widths were taken into account in terms of Gaussian profiles determined from a fit of the measured local oscillator spectrum. In this way, the central

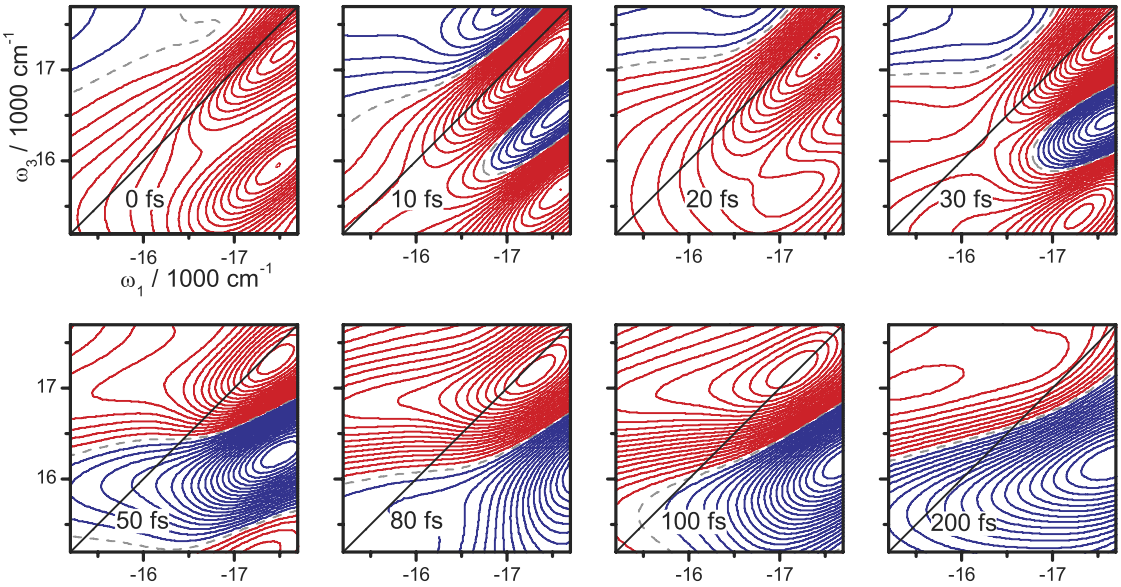

FIG. 8. Simulated electronic 2D spectra of okenone, the carotenoid in LH2 *M. pur.* The employed values of t_2 are indicated in the panels. Line coloring follows the same conventions as described in Fig. 3.

frequency $\omega_0 = 16\,275\ \text{cm}^{-1}$ and a FWHM of $1612\ \text{cm}^{-1}$ were obtained. As the fitted curve corresponds to the squared pulse profile, multiplication of the FWHM with a factor of $\sqrt{2}$ was required to obtain the FWHM of the single pulses with a value of $2280\ \text{cm}^{-1}$.

In the real part of the sum of all calculated response function contributions after convolution with the pulses, an intensive positive-valued diagonal peak in the region of $\omega_1 = -17\,500\ \text{cm}^{-1}$ and $\omega_3 = 17\,500\ \text{cm}^{-1}$ appears at all population times t_2 up to 100 fs, starting from $t_2 = 0$ fs. This peak mainly stems from the rephasing GSB contribution. Furthermore, below the diagonal at $\omega_1 = -17\,500\ \text{cm}^{-1}$ and $\omega_3 = 16\,000\ \text{cm}^{-1}$, a crosspeak from the rephasing GSB contribution is found, which stems from vibrational effects. This initially oval peak becomes butterfly shaped with a nodal line separating positive and negative regions at $t_2 = 10$ fs, whereas at $t_2 = 20$ fs, it becomes completely positive again. At $t_2 = 30$ fs, a modified shape of the vibrational crosspeak below the diagonal from the rephasing GSB contribution in combination with a rise of the rephasing SE contribution and the negative-valued rephasing ESA contribution leads to a localization of the crosspeak close to $\omega_1 = -18\,000\ \text{cm}^{-1}$ and $\omega_3 = 15\,500\ \text{cm}^{-1}$. From $t_2 = 50$ fs, the ESA contribution starts to obscure the latter. At $t_2 = 80$ fs, the negative ESA peak covers a broad energetic range below the diagonal. This tendency becomes even more pronounced at $t_2 = 100$ fs and $t_2 = 200$ fs, where the ESA peak pushes the diagonal peak almost completely above the diagonal.

Different from the measured 2D-spectra, the upper diagonal peak at $t_2 = 0$–30 fs is missing in the calculated 2D-spectra shown in Fig. 8, most likely due to the fact that the spectral phase of the pulses was considered as flat in the calculations. When comparing the spectra from experiment (Fig. 4) and simulation (Fig. 8) at $t_2 = 30$ fs, it becomes apparent that the experimentally obtained cross peak, which we identified as an indication of $S_2 \rightarrow Q_x$ energy transfer, is missing in simulations. Considering that the simulations only incorporate the okenone-part of the spectrum, this missing cross peak confirms our assignment to energy transfer to Q_x. 2D-ES elucidates why carotenoid to BCh l energy transfer pathways are difficult to analyze in pump-probe spectroscopy.[24,82] The corresponding cross peak coincides with a recurring negative carotenoid feature (see $t_2 = 30$ fs and $t_2 = 10$ fs spectrum in Fig. 8). Additionally, $S_2 \rightarrow Q_x$ energy transfer is overlaid with ESA from S_1, making it only observable within the ultrashort lifetime of S_2, i.e., only during 55 fs in LH2 *M. pur.*

V. CONCLUSIONS AND OUTLOOK

In this work, we have shown that vibronic coupling mechanism describes several central aspects of the carotenoid to BChl ($S_2 \rightarrow Q_x$) energy transfer dynamics. To reproduce experimentally observed energy transfer rates, this mechanism requires only moderate coupling constants J close to $100\ \text{cm}^{-1}$. This value is in excellent agreement with structure-based calculations and, within the vibronic model, it reproduces experimental absorption spectra well. The main mechanism, which dramatically speeds up energy transfer, is the deposition of excess excitation energy into the ground state vibrations of the carotenoid (donor) molecule.

The investigated carotenoid-BChl system is an extreme case of a heterodimer, meaning that donor (carotenoid) and acceptor (BChl) differ in transition energies and HR-factor. Future studies will test the vibronic coupling mechanism on energy transferring dimers where the spectroscopic properties are more alike, such as perylene bisimide dyads.[83] In such systems, both donor and acceptor show strong electron-phonon coupling, which should make vibronic effects in energy transfer dynamics even more pronounced. Another highly promising class of systems is bulk heterojunction solar cells, where vibronic coupling between donor and acceptor was recently suggested to be the mechanism behind ultrafast electron transfer.[84]

ACKNOWLEDGMENTS

The authors wish to thank Ana Moore for providing the dyad sample and Heiko Lokstein for fruitful discussion. Funding by the Austrian Science Fund (FWF): START Project No. Y 631-N27 (J.H. and C.N.L.), the CZE—Aus Mobility Grant (Grant No. 7AMB14AT007, CZ 05/2014) (J.H., C.N.L., V.P., J.S., F.S., and T.M.), and by the Czech Science Foundation (GACR) Grant No. 14-25752S (V.P., J.S., F.S., and T.M.) is acknowledged. V.P. acknowledges support from GAUK (Grant No. 2940214). R.J.C. and L.J.C. acknowledge funding by BBSRC.

APPENDIX: RESPONSE FUNCTIONS

In this appendix, the response functions used to calculated the Car 2D-spectrum are specified. The rephasing GSB term with population of S_2 and a decay due to intramolecular transfer to S_1 is given as

$$\begin{aligned} R_{3g,S_2}(\tau_3,\tau_2,\tau_1) = {} & \left|\mu_{S_0S_2}\right|^4 \exp(i\omega_{S_2S_0}\tau_1 - i\omega_{S_2S_0}\tau_3)\exp\left(-\Gamma_{S_2}\tau_1 - \Gamma_{S_2}\tau_3\right)\exp(-g^*_{S_2S_2}(\tau_1) + g^*_{S_2S_2}(\tau_2) - g_{S_2S_2}(\tau_3) \\ & - g^*_{S_2S_2}(\tau_1+\tau_2) - g^*_{S_2S_2}(\tau_2+\tau_3) + g^*_{S_2S_2}(\tau_1+\tau_2+\tau_3)). \end{aligned} \tag{A1}$$

The rephasing SE component with decay of the S_2 component due to intramolecular transfer to S_1 reads

$$\begin{aligned} R_{2g,S_2}(\tau_3,\tau_2,\tau_1) = {} & \left|\mu_{S_0S_2}\right|^4 \exp(i\omega_{S_2S_0}\tau_1 - i\omega_{S_2S_0}\tau_3)\exp\left(-\Gamma_{S_2}\tau_1 - \Gamma_{S_2}\tau_3\right)\exp(-g^*_{S_2S_2}(\tau_1) + g_{S_2S_2}(\tau_2) - g^*_{S_2S_2}(\tau_3) \\ & - g^*_{S_2S_2}(\tau_1+\tau_2) - g_{S_2S_2}(\tau_2+\tau_3) + g^*_{S_2S_2}(\tau_1+\tau_2+\tau_3))\exp(-k_{S_2\to S_1}\tau_2). \end{aligned} \tag{A2}$$

For the rephasing ESA component with population transfer from S_2 to S_1 and subsequent excitation to a higher excited state, one obtains

$$\begin{aligned} R^*_{1f,S_2\to S_1}(\tau_3,\tau_2,\tau_1) = {} & -\left|\mu_{S_0S_2}\right|^2\left|\mu_{S_1S_n}\right|^2 \exp(i\omega_{S_2S_0}\tau_1 - i\omega_{S_nS_1}\tau_3)\exp\left(-\Gamma_{S_2}\tau_1 - \Gamma_{S_1}\tau_3\right)\exp(-g^*_{S_2S_2}(\tau_1) - g_{S_2S_1}(\tau_2) \\ & - g_{S_1S_1}(\tau_3) + g^*_{S_2S_1}(\tau_1+\tau_2) + g_{S_2S_1}(\tau_2+\tau_3) - g^*_{S_2S_1}(\tau_1+\tau_2+\tau_3))\exp(g_{S_nS_2}(\tau_2) \\ & + 2g_{S_nS_1}(\tau_3) - g^*_{S_nS_2}(\tau_1+\tau_2) - g_{S_nS_2}(\tau_2+\tau_3) + g^*_{S_nS_2}(\tau_1+\tau_2+\tau_3) - g_{S_nS_n}(\tau_3)) \\ & \times k_{S_2\to S_1}\int_0^{\tau_2} d\tau \exp(-k_{S_2\to S_1}\tau)\exp(2i\Im(g_{S_2S_1}(\tau_2-\tau) - g_{S_1S_1}(\tau_2-\tau) + g_{S_1S_1}(\tau_2-\tau+\tau_3) \\ & - g_{S_2S_1}(\tau_2-\tau+\tau_3)))\exp(2i\Im(g_{S_nS_1}(\tau_2-\tau) \\ & - g_{S_nS_2}(\tau_2-\tau) + g_{S_nS_2}(\tau_2-\tau+\tau_3) - g_{S_nS_1}(\tau_2-\tau+\tau_3))). \end{aligned} \tag{A3}$$

The nonrephasing response functions of GSB-, SE-, and ESA-types read

$$\begin{aligned} R_{4g,S_2}(\tau_3,\tau_2,\tau_1) = {} & \left|\mu_{S_0S_2}\right|^4 \exp(-i\omega_{S_2S_0}\tau_1 - i\omega_{S_2S_0}\tau_3)\exp\left(-\Gamma_{S_2}\tau_1 - \Gamma_{S_2}\tau_3\right)\exp(-g_{S_2S_2}(\tau_1) - g_{S_2S_2}(\tau_2) - g_{S_2S_2}(\tau_3) \\ & + g_{S_2S_2}(\tau_1+\tau_2) + g_{S_2S_2}(\tau_2+\tau_3) - g_{S_2S_2}(\tau_1+\tau_2+\tau_3)), \end{aligned} \tag{A4}$$

$$\begin{aligned} R_{1g,S_2}(\tau_3,\tau_2,\tau_1) = {} & \left|\mu_{S_0S_2}\right|^4 \exp(-i\omega_{S_2S_0}\tau_1 - i\omega_{S_2S_0}\tau_3)\exp\left(-\Gamma_{S_2}\tau_1 - \Gamma_{S_2}\tau_3\right)\exp(-g_{S_2S_2}(\tau_1) - g^*_{S_2S_2}(\tau_2) - g^*_{S_2S_2}(\tau_3) \\ & + g_{S_2S_2}(\tau_1+\tau_2) + g^*_{S_2S_2}(\tau_2+\tau_3) - g_{S_2S_2}(\tau_1+\tau_2+\tau_3))\exp(-k_{S_2\to S_1}\tau_2), \end{aligned} \tag{A5}$$

and

$$\begin{aligned} R^*_{2f,S_2\to S_1}(\tau_3,\tau_2,\tau_1) = {} & -\left|\mu_{S_0S_2}\right|^2\left|\mu_{S_1S_n}\right|^2 \exp(-i\omega_{S_2S_0}\tau_1 - i\omega_{S_nS_1}\tau_3)\exp\left(-\Gamma_{S_2}\tau_1 - \Gamma_{S_1}\tau_3\right)\exp(-g_{S_2S_2}(\tau_1) \\ & + g^*_{S_2S_1}(\tau_2) - g_{S_1S_1}(\tau_3) - g_{S_2S_1}(\tau_1+\tau_2) - g^*_{S_2S_1}(\tau_2+\tau_3) + g_{S_2S_1}(\tau_1+\tau_2+\tau_3)) \\ & \times \exp(-g^*_{S_nS_2}(\tau_2) + 2g_{S_nS_1}(\tau_3) + g_{S_nS_2}(\tau_1+\tau_2) + g^*_{S_nS_2}(\tau_2+\tau_3) \\ & - g_{S_nS_2}(\tau_1+\tau_2+\tau_3) - g_{S_nS_n}(\tau_3))k_{S_2\to S_1}\int_0^{\tau_2} d\tau \exp(-k_{S_2\to S_1}\tau) \\ & \times \exp(2i\Im(g_{S_2S_1}(\tau_2-\tau) - g_{S_1S_1}(\tau_2-\tau) + g_{S_1S_1}(\tau_2-\tau+\tau_3) - g_{S_2S_1}(\tau_2-\tau+\tau_3))) \\ & \times \exp(2i\Im(g_{S_nS_1}(\tau_2-\tau) - g_{S_nS_2}(\tau_2-\tau) + g_{S_nS_2}(\tau_2-\tau+\tau_3) - g_{S_nS_1}(\tau_2-\tau+\tau_3))). \end{aligned} \tag{A6}$$

[1]T. Renger, V. May, and O. Kuhn, Phys. Rep. **343**, 137 (2001).
[2]H. Lokstein and B. Grimm, *eLS* (John Wiley & Sons, 2013).
[3]V. Sundstrom, "Biophotonics: Spectroscopy, imaging, sensing, and manipulation," *NATO Science for Peace and Security Series B-Physics and Biophysics*, edited by B. DiBartolo and J. Collins (Springer, 2011), pp. 219–236.
[4]R. E. Blankenship, *Molecular Mechanisms of Photosynthesis*, 2nd ed. (Wiley-Blackwell, Oxford, UK, 2014).
[5]T. Polívka and V. Sundström, Chem. Rev. **104**, 2021 (2004).
[6]T. Polivka and V. Sundstrom, Chem. Phys. Lett. **477**, 1 (2009).
[7]E. E. Ostroumov, R. M. Mulvaney, R. J. Cogdell, and G. D. Scholes, Science **340**, 52 (2013).

[8]E. E. Ostroumov, R. M. Mulvaney, J. M. Anna, R. J. Cogdell, and G. D. Scholes, J. Phys. Chem. B **117**, 11349 (2013).
[9]P. Tavan and K. Schulten, Phys. Rev. B **36**, 4337 (1987).
[10]J. P. Zhang, T. Inaba, Y. Watanabe, and Y. Koyama, Chem. Phys. Lett. **332**, 351 (2000).
[11]G. Cerullo, D. Polli, G. Lanzani, S. De Silvestri, H. Hashimoto, and R. J. Cogdell, "Photosynthetic light harvesting by carotenoids: Detection of an intermediate excited state," Science **298**, 2395 (2002).
[12]E. Ostroumov, M. G. Müller, C. M. Marian, M. Kleinschmidt, and A. R. Holzwarth, Phys. Rev. Lett. **103**, 1 (2009).
[13]M. S. Marek, T. Buckup, and M. Motzkus, J. Phys. Chem. B **115**, 8328 (2011).
[14]M. Maiuri, D. Polli, D. Brida, L. Luer, A. M. LaFountain, M. Fuciman, R. J. Cogdell, H. A. Frank, and G. Cerullo, Phys. Chem. Chem. Phys. **14**, 6312 (2012).
[15]D. Kosumi, M. Komukai, H. Hashimoto, and M. Yoshizawa, Phys. Rev. Lett. **95**, 213601 (2005).
[16]N. Christensson, F. Milota, A. Nemeth, J. Sperling, H. F. Kauffmann, T. Pullerits, and J. Hauer, J. Phys. Chem. B **113**, 16409 (2009).
[17]N. Christensson, F. Milota, A. Nemeth, I. Pugliesi, E. Riedle, J. Sperling, T. Pullerits, H. Kauffmann, and J. Hauer, J. Phys. Chem. Lett. **1**, 3366 (2010).
[18]M. Liebel, C. Schnedermann, and P. Kukura, Phys. Rev. Lett. **112**, 198302 (2014).
[19]T. Polivka and H. A. Frank, Acc. Chem. Res. **43**, 1125 (2010).
[20]R. S. Knox, J. Photochem. Photobiol., B **49**, 81 (1999).
[21]M. Gouterman, J. Chem. Phys. **30**, 1139 (1959).
[22]V. N. Nemykin, R. G. Hadt, R. V. Belosludov, H. Mizuseki, and Y. Kawazoe, J. Phys. Chem. A **111**, 12901 (2007).
[23]T. Mancal, N. Christensson, V. Lukes, F. Milota, O. Bixner, H. F. Kauffmann, and J. Hauer, J. Phys. Chem. Lett. **3**, 1497 (2012).
[24]A. N. Macpherson, P. A. Liddell, D. Kuciauskas, D. Tatman, T. Gillbro, D. Gust, T. A. Moore, and A. L. Moore, J. Phys. Chem. B **106**, 9424 (2002).
[25]J. Savolainen, N. Dijkhuizen, R. Fanciulli, P. A. Liddell, D. Gust, T. A. Moore, A. L. Moore, J. Hauer, T. Buckup, M. Motzkus, and J. L. Herek, J. Phys. Chem. B **112**, 2678 (2008).
[26]T. H. P. Brotosudarmo, A. M. Collins, A. Gall, A. W. Roszak, A. T. Gardiner, R. E. Blankenship, and R. J. Cogdell, Biochem. J. **440**, 51 (2011).
[27]F. Milota, C. N. Lincoln, and J. Hauer, Opt. Express **21**, 15904 (2013).
[28]N. Christensson, F. Milota, J. Hauer, J. Sperling, O. Bixner, A. Nemeth, and H. F. Kauffmann, J. Phys. Chem. B **115**, 5383 (2011).
[29]J. Piel, E. Riedle, L. Gundlach, R. Ernstorfer, and R. Eichberger, Opt. Lett. **31**, 1289 (2006).
[30]M. L. Cowan, J. P. Ogilvie, and R. J. D. Miller, Chem. Phys. Lett. **386**, 184 (2004).
[31]T. Brixner, T. Mancal, I. V. Stiopkin, and G. R. Fleming, J. Chem. Phys. **121**, 4221 (2004).
[32]F. Milota, J. Sperling, A. Nemeth, and H. F. Kauffmann, Chem. Phys. **357**, 45 (2009).
[33]M. J. Tauber, R. A. Mathies, X. Y. Chen, and S. E. Bradforth, Rev. Sci. Instrum. **74**, 4958 (2003).
[34]S. Mukamel, *Principles of Nonlinear Optical Spectroscopy* (Oxford University Press, New York, 1995).
[35]J. Seibt and T. Pullerits, J. Chem. Phys. **141**, 114106 (2014).
[36]T. Mančal, J. Dostál, J. Pšenčík, and D. Zigmantas, Can. J. Chem. **92**, 135 (2014).
[37]T. Brixner, T. Mančal, I. V. Stiopkin, and G. R. Fleming, J. Chem. Phys. **121**, 4221 (2004).
[38]S. Tretiak, C. Middleton, V. Chernyak, and S. Mukamel, J. Phys. Chem. B **104**, 9540 (2000).
[39]V. Perlik, C. Lincoln, F. Sanda, and J. Hauer, J. Phys. Chem. Lett. **5**, 404 (2014).
[40]L. D. Landau and E. Teller, Phys. Z. Sowjetunion **10**, 34 (1936).
[41]F. Sanda, J. Phys. A: Math. Gen. **35**, 5815 (2002).
[42]T. Renger and R. A. Marcus, J. Chem. Phys. **116**, 9997 (2002).
[43]D. Gust, T. A. Moore, A. L. Moore, C. Devadoss, P. A. Liddell, R. Hermant, R. A. Nieman, L. J. Demanche, J. M. DeGraziano, and I. Gouni, J. Am. Chem. Soc. **114**, 3590 (1992).
[44]J. Savolainen, R. Fanciulli, N. Dijkhuizen, A. L. Moore, J. Hauer, T. Buckup, M. Motzkus, and J. L. Herek, Proc. Natl. Acad. Sci. U. S. A. **105**, 7641 (2008).
[45]M. Z. Papiz, S. M. Prince, T. Howard, R. J. Cogdell, and N. W. Isaacs, J. Mol. Biol. **326**, 1523 (2003).
[46]G. McDermott, S. M. Prince, A. A. Freer, A. M. Hawthornthwaite-Lawless, M. Z. Papiz, R. J. Cogdell, and N. W. Isaacs, Nature **374**, 517 (1995).
[47]L. J. Cranston, A. W. Roszak, and R. J. Cogdell, Acta Crystallogr., Sect. F **70**, 808 (2014).
[48]D. Polli, G. Cerullo, G. Lanzani, S. De Silvestri, H. Hashimoto, and R. J. Cogdell, Biophys. J. **90**, 2486 (2006).
[49]M. Sugisaki, M. Fujiwara, D. Kosumi, R. Fujii, M. Nango, R. J. Cogdell, and H. Hashimoto, Phys. Rev. B **81**, 245112 (2010).
[50]G. Cerullo, G. Lanzani, M. Zavelani-Rossi, and S. De Silvestri, Phys. Rev. B **63**, 241104(R) (2001).
[51]J. Hauer, H. Skenderovic, K. L. Kompa, and M. Motzkus, Chem. Phys. Lett. **421**, 523 (2006).
[52]H. Hashimoto, M. Sugisaki, and M. Yoshizawa, Biochim. Biophys. Acta, Bioenerg. **1847**, 69 (2015).
[53]R. Fujii, C. H. Chen, T. Mizoguchi, and Y. Koyama, Spectrochim. Acta, Part A **54**, 727 (1998).
[54]T. M. Cotton and R. P. Vanduyne, J. Am. Chem. Soc. **103**, 6020 (1981).
[55]D. M. Jonas, Annu. Rev. Phys. Chem. **54**, 425 (2003).
[56]A. Nemeth, F. Milota, T. Mancal, V. Lukes, J. Hauer, H. F. Kauffmann, and J. Sperling, J. Chem. Phys. **132**, 184514 (2010).
[57]D. B. Turner, K. E. Wilk, P. M. G. Curmi, and G. D. Scholes, J. Phys. Chem. Lett. **2**, 1904 (2011).
[58]V. Butkus, D. Zigmantas, L. Valkunas, and D. Abramavicius, Chem. Phys. Lett. **545**, 40 (2012).
[59]L. Valkunas, D. Abramavicius, and T. Mančal, *Molecular Excitation Dynamics and Relaxation: Quantum Theory and Spectroscopy* (Wiley-VCH Verlag, Berlin, 2013).
[60]N. Christensson, Y. Avlasevich, A. Yartsev, K. Mullen, T. Pascher, and T. Pullerits, J. Chem. Phys. **132**, 174508 (2010).
[61]P. O. Andersson, R. J. Cogdell, and T. Gillbro, Chem. Phys. **210**, 195 (1996).
[62]H. Nagae, T. Kakitani, T. Katoh, and M. Mimuro, J. Chem. Phys. **98**, 8012 (1993).
[63]H. van Amerongen, L. Valkunas, and R. van Grondelle, *Photosynthetic Excitons* (World Scientific, Singapore, 2000).
[64]Y. C. Cheng and R. J. Silbey, Phys. Rev. Lett. **96**, 028103 (2006).
[65]A. Ishizaki and G. R. Fleming, J. Chem. Phys. **130**, 234111 (2009).
[66]N. Christensson, H. F. Kauffmann, T. Pullerits, and T. Mančal, J. Phys. Chem. B **116**, 7449 (2012).
[67]V. Tiwari, W. K. Peters, and D. M. Jonas, Proc. Natl. Acad. Sci. U. S. A. **110**, 1203 (2013).
[68]A. W. Chin, J. Prior, R. Rosenbach, F. Caycedo-Soler, S. F. Huelga, and M. B. Plenio, Nat. Phys. **9**, 113 (2013).
[69]A. Chenu, N. Christensson, H. F. Kauffmann, and T. Mančal, Sci. Rep. **3**, 2029 (2013).
[70]A. Ishizaki and G. R. Fleming, J. Chem. Phys. **130**, 234110 (2009).
[71]B. P. Krueger, G. D. Scholes, and G. R. Fleming, J. Phys. Chem. B **102**, 5378 (1998).
[72]D. Zigmantas, E. L. Read, T. Mancal, T. Brixner, A. T. Gardiner, R. J. Cogdell, and G. R. Fleming, Proc. Natl. Acad. Sci. U. S. A. **103**, 12672 (2006).
[73]S. Mukamel and V. Rupasov, Chem. Phys. Lett. **242**, 17 (1995).
[74]V. May and O. Kühn, *Charge and Energy Transfer Dynamics in Molecular Systems* (Wiley-VCH Verlag, Berlin, 2000).
[75]G. D. Scholes, Annu. Rev. Phys. Chem. **54**, 57 (2003).
[76]D. Beljonne, C. Curutchet, G. D. Scholes, and R. J. Silbey, J. Phys. Chem. B **113**, 6583 (2009).
[77]J. M. Womick and A. M. Moran, J. Phys. Chem. B **115**, 1347 (2011).
[78]N. Christensson, K. Žídek, N. C. M. Magdaong, A. M. LaFountain, H. A. Frank, and D. Zigmantas, J. Phys. Chem. B **117**, 11209 (2013).
[79]N. Christensson, F. Milota, A. Nemeth, J. Sperling, H. F. Kauffmann, T. Pullerits, and J. Hauer, J. Phys. Chem. B **113**, 16409 (2009).
[80]M. Sugisaki, K. Yanagi, R. Cogdell, and H. Hashimoto, Phys. Rev. B **75**, 155110 (2007).
[81]N. Christensson, T. Polivka, A. Yartsev, and T. Pullerits, Phys. Rev. B **79**, 245118 (2009).
[82]H. Cong, D. M. Niedzwiedzki, G. N. Gibson, A. M. LaFountain, R. M. Kelsh, A. T. Gardiner, R. J. Cogdell, and H. A. Frank, J. Phys. Chem. B **112**, 10689 (2008).
[83]H. Langhals, A. J. Esterbauer, A. Walter, E. Riedle, and I. Pugliesi, J. Am. Chem. Soc. **132**, 16777 (2010).
[84]S. M. Falke, C. A. Rozzi, D. Brida, M. Maiuri, M. Amato, E. Sommer, A. De Sio, A. Rubio, G. Cerullo, E. Molinari, and C. Lienau, Science **344**, 1001 (2014).